Research Paper

GEOSPHERE

GEOSPHERE; v. 15, no. 1

https://doi.org/10.1130/GES01670.1

12 figures; 4 tables

CORRESPONDENCE: wetmore@usf.edu

CITATION: Wetmore, P.H., Malservisi, R., Fletcher, J.M., Alsleben, H., Wilson, J., Callihan, S., Springer, A., González-Yajimovich, O., and Gold, P.O., 2019, Slip history and the role of the Agua Blanca fault in the tectonics of the North American–Pacific plate boundary of southern California, USA and Baja California, Mexico: Geosphere, v. 15, no. 1, p. 119–145, https://doi.org/10.1130/GES01670.1.

Science Editor: Raymond M. Russo
Associate Editor: Jose Miguel Hurtado

Received 11 January 2018
Revision received 5 June 2018
Accepted 3 October 2018
Published online 5 December 2018

Slip history and the role of the Agua Blanca fault in the tectonics of the North American–Pacific plate boundary of southern California, USA and Baja California, Mexico

Paul H. Wetmore[1], Rocco Malservisi[1], John M. Fletcher[2], Helge Alsleben[3], James Wilson[1], Sean Callihan[1], Adam Springer[1], Oscar González-Yajimovich[4], and Peter O. Gold[5]

[1]Department of Geology, University of South Florida, Tampa, Florida 33620, USA
[2]Departamento de Geología, Centro de Investigación Científica y de Educación Superior de Ensenada, Carretera Tijuana-Ensenada No. 3918, Zona Playitas, Ensenada, Baja California, Mexico C.P. 22860
[3]School of Geology, Energy and the Environment, Texas Christian University, Fort Worth, Texas 76129, USA
[4]Universidad Autónoma de Baja California, Ensenada, Baja California, Mexico C.P. 22860
[5]Jackson School of Geosciences, University of Texas at Austin, Austin, Texas 78712, USA

ABSTRACT

The Agua Blanca fault (ABF) is a west-northwest–trending oblique dextral-normal fault that defines the southern boundary of the Big Bend domain (BBD) of the Pacific–North American plate margin and the northern limit to the rigid Baja California microplate. Our geologic and geodetic studies demonstrate that finite slip on the ABF reaches a maximum of ~11 km of nearly pure dextral strike slip in central portions of the fault, whereas the magnitude of displacement decreases and the proportion of extension increases in the sections to both the east and west. To the east, the ABF appears to die out before crossing into the San Pedro Mártir fault, with slip transferred onto a series of more northerly-trending, dip-slip faults. To the west, the ABF bifurcates to form the Santo Tomás fault (STF) in the Valle Santo Tomás section, where we measure ~5 km of dextral offset for the ABF and ~3 km estimated offset on the STF. And we report a measurement of ~7 km of dextral offset on the ABF in the Punta Banda section. Small offset faults proximal to the ABF likely accommodate additional dextral shear in the western sections of the fault. The STF in the Valle Santo Tomás section and the ABF in the Punta Banda section exhibit 0.58 and 0.65 km of extensional heave, or ~7% and 10% of the total displacement in each section, respectively. Block modeling based on geodetic data agrees well with geologic determinations of slip direction and reveals near perfect alignment of the central ABF with the relative block motion vectors and increased proportions of fault-perpendicular extension to both the east (3%–10%) and west (5%–13%). Based on our new estimates of the total offsets combined with existing slip rates, the ABF likely initiated between 3.3 and 1.5 Ma. This age range overlaps with those reported for other faults within the area of the BBD southwest of the San Andreas fault. The ABF has a more westerly orientation than the transpressional restraining-bend segment of the San Andreas, yet it accommodates transtensional shearing. This requires a reevaluation of the processes that control transpression and transtension within the BBD.

INTRODUCTION

The North American–Pacific plate boundary through the United States and Mexico is composed of a complex system of faults whose kinematics and geographic distributions allow for a subdivision into three domains (Fig. 1; Fletcher et al., 2014). From north to south, these include the San Andreas, Big Bend, and Gulf of California domains. The San Andreas domain includes the San Andreas fault (SAF) along with an anastomosing network of faults following the central California coast and includes domains of partitioned plate motion in the Walker Lane, Great Basin, and Rio Grande rift. The Big Bend domain (BBD), located between the Garlock fault and the Agua Blanca fault (ABF), is composed of a network of faults stretching across a ~500-km-wide region with the SAF at its approximate center. The faults of the Mojave section of the Eastern California shear zone (ECSZ) are present to the northeast, and a network of faults identified by Legg et al. (1991) as the Southern California shear zone (SCSZ) is present to the southwest of the SAF. The SCSZ predominantly consists of northwest-trending dextral strike-slip faults that initiated in the Quaternary (e.g., Steely et al., 2009; Janecke et al., 2010; Dorsey et al., 2012). The Gulf of California domain, located to the south of the ABF, includes a suite of en echelon transform faults with short spreading centers in the steps. Unlike the two northern domains, the vast majority of the plate boundary shear (~90%; Plattner et al., 2007, 2009) is confined to these transform faults. The remaining plate motion in this domain is accommodated by active faults west of the Baja California microplate (Plattner et al., 2007, 2009).

The ABF defines the northern limit of the Baja California microplate and the southern limit of the BBD. It is a unique structure within the North American–Pacific plate boundary zone of southern and Baja California in that it is a predominantly dextral strike-slip fault (e.g., Allen et al., 1960 and this study) with a trace oriented at a high angle (276° to 302°) to the regional maximum horizontal compressive stress (Fig. 1; Townend and Zoback, 2004). Its strike is,

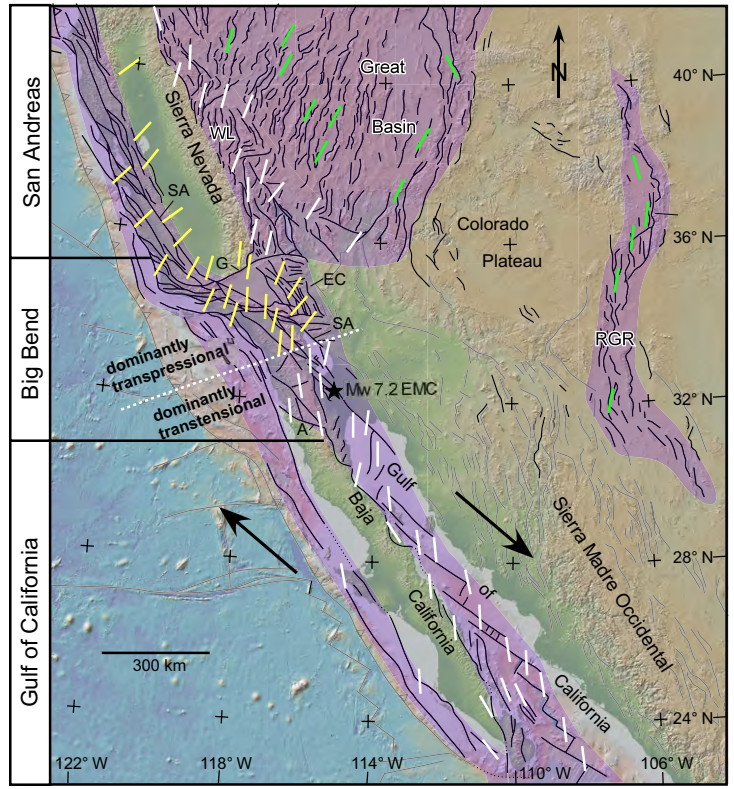

Figure 1. Tectonic map of western North America showing the main shear zones (purple shading) that comprise the Pacific–North American plate margin. Simplified fault traces include Quaternary faults (black; simplified from U.S. Geological Survey, 2006; and regional mapping in western Mexico by Fletcher et al. [2014]) and inactive Neogene faults (gray; simplified from Muehlberger, 1996). Maximum horizontal compressive stress shown by thick horizontal lines defines regions of transtension (white), transpression (yellow), and extension (green) (simplified from World Stress Map database; Heidbach et al., 2010). In this study, the plate margin is divided into three main domains: Gulf of California, Big Bend, and San Andreas. Transtensive relative plate motion is accommodated in a narrow belt in the Gulf of California with minor slip (~5 mm/yr) occurring in the continental shelf west of Baja California (Dixon et al., 2000). In the Big Bend domain, plate margin shearing changes from transtensive to transpressive and bifurcates into the north-northwest–trending eastern California shear zone (EC) and a network of west-northwest–striking faults that includes the Big Bend segment of the San Andreas fault. In the San Andreas domain, relative plate motion is partitioned into the transpressive San Andreas fault system (SA), transtensive Walker lane shear zone (WL), and extension in the Great Basin. Minor extension is also partitioned into the Rio Grande Rift (RGR), which forms an isolated belt of shearing that overlaps with portions of all three domains. Black star marks epicenter of the 4 April 2010 Mw 7.2 El Mayor–Cucapah earthquake located within the Big Bend domain. A—Agua Blanca fault; G—Garlock fault. Figure modified from Fletcher et al. (2014).

in fact, as much as 18° more westerly than the San Andreas fault through the Big Bend segment, which is strongly transpressional, due to the left-stepping restraining geometry of the bend (e.g., Hill and Dibblee, 1953). However, significant differences in the nature of shearing across faults with similar geometries demonstrate that relative plate motion alone cannot explain the nature of deformation along the plate margin.

In this study, we present new mapping and geodetic modeling that demonstrate that the ABF has been, and is currently, dominated by dextral strike-slip motion with a subordinate component of fault-perpendicular extension along its entire length. Addressing the apparent discrepancy between the stress trajectories and fault kinematics in this part of the BBD is a primary motivation for this study as we: (1) seek to demonstrate the recent and long-term slip history along the ABF, and (2) place this slip history into the context of the broader regional tectonic setting.

The following sections of this study include: a brief description of the relevant regional geology; detailed descriptions of the ABF and subordinate faults, with particular focus on the total offset and kinematics; a reanalysis of existing geodetic data and new block modeling to better constrain the active kinematics of the ABF; and a detailed discussion of the slip history of the ABF and its role within the broader North American–Pacific plate boundary.

GEOLOGIC BACKGROUND

Regional Tectonic Setting

The dominant tectonic setting of the North American–Pacific plate boundary in southern California and northern Baja California is deformation associated with the Big Bend in the SAF. Initiation of the Big Bend at ca. 6 Ma (e.g., Crowell, 1982, 2003; Ingersoll and Rumelhart, 1999; Kellogg and Minor, 2005) happened penecontemporaneously with the jump of the southern SAF to the east of the Peninsular Ranges, and the opening of the Gulf of California (Oskin and Stock, 2003). Since that time, transpression and contraction has propagated southward from the SAF (e.g., Rockwell, 1983; Yeats et al., 1994), and the northern end of the Baja California microplate has been broken up by a series of dextral strike-slip faults (e.g., San Jacinto, Elsinore, and San Miguel–Vallecitos faults; see Fig. 2A). The ABF represents the bounding structure juxtaposing the disrupted northern section of the Baja California microplate from the rigid central portion (Plattner et al., 2007, 2009).

Faults within the part of the BBD located to the southwest of the SAF exhibit a wide variety of orientations and kinematics. However, the latter are typically governed by the former because faults trending northwest are characteristically dextral strike slip (e.g., Elsinore and San Jacinto faults), whereas those oriented with more northerly trends (e.g., Sierra Juarez and Cañada David faults) tend to be more dominantly extensional and/or transtensional (e.g., Mueller and Rockwell, 1995; Fletcher and Spelz, 2009; Janecke et al., 2010). The few faults with westerly or west-northwest trends (e.g., Whittier fault, ~295°; Herzog, 1998) tend

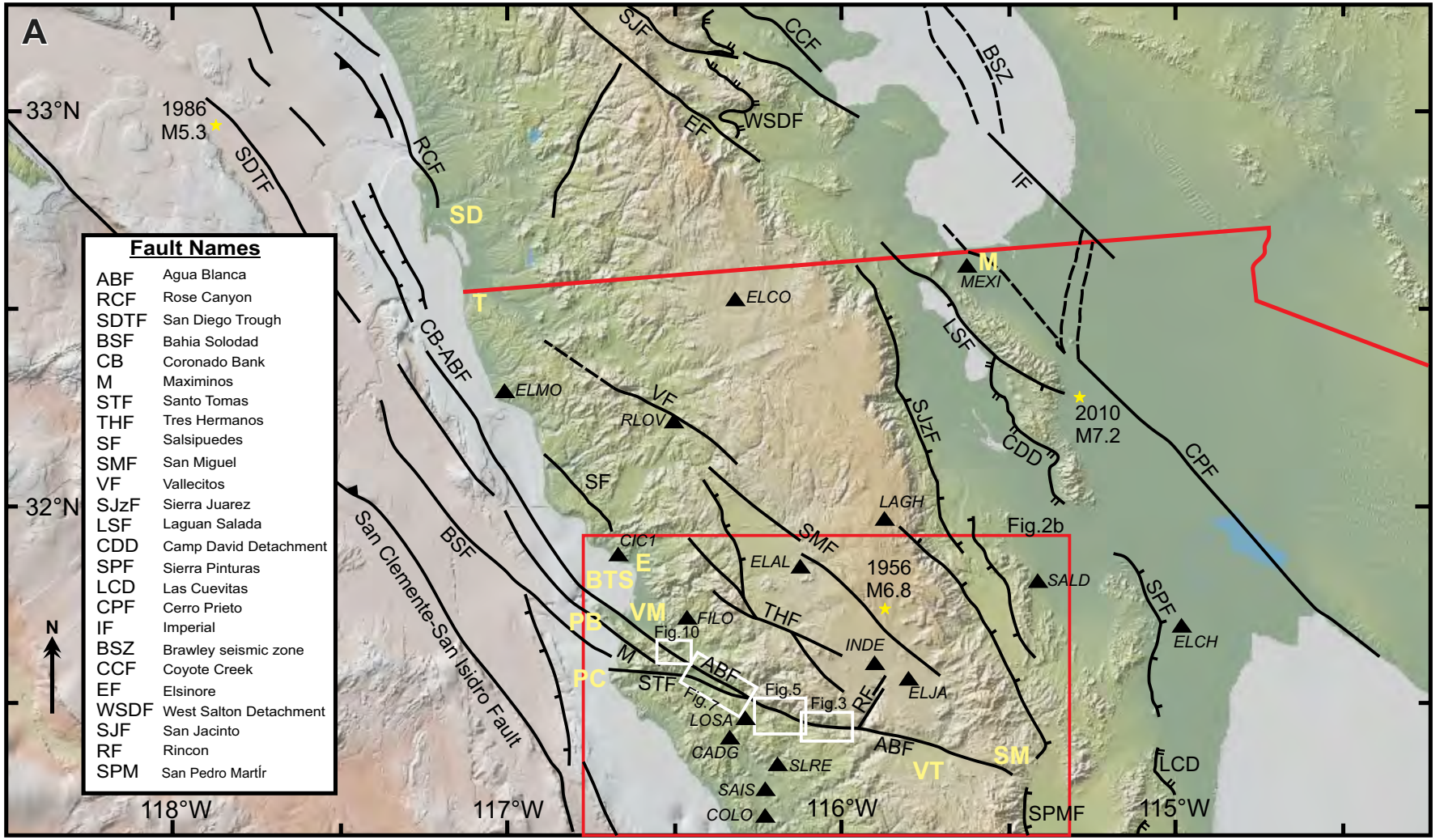

Figure 2 (*on this and following page*). (A) Fault map of southern California, northernmost Baja California, and the Inner Continental Borderlands overlain on a colored digital elevation model. Fault locations are derived from Legg et al. (1991), Suarez-Vidal et al. (1991), Fisher et al. (2009), Ryan et al. (2009), and Janecke et al. (2010). Yellow letters represent the locations of towns and geographic locations alluded to in the text; SD—San Diego; T—Tijuana; M—Mexicali; E—Ensenada; PB—Punta Banda; PC—Punta China; VT—Valle Trinidad; SM—San Matiás Pass; BTS—Bahia Todos Santos; VM—Valle Maneadero. Yellow stars depict the locations of significant recent earthquakes with year and magnitude.

to be contractional to transpressional strike slip, and they are largely confined to the area just south of the Transverse Ranges. A boundary appears to exist that divides this part of the BBD into regions of dominantly transpressional faults to the north from dominantly transtensional faults to the south (Fig. 1). This line stretches from the northern half of the Salton Sea southwest through San Diego, continuing into the inner Continental Borderlands. Northwest-trending faults to the north of this line tend to have a greater number of left bends and steps, whereas those to the south have a greater number of right steps and bends. This holds true for the major structures on land as well as the faulting offshore in Inner Continental Borderlands (e.g., Legg et al., 1991; Ryan et al., 2009).

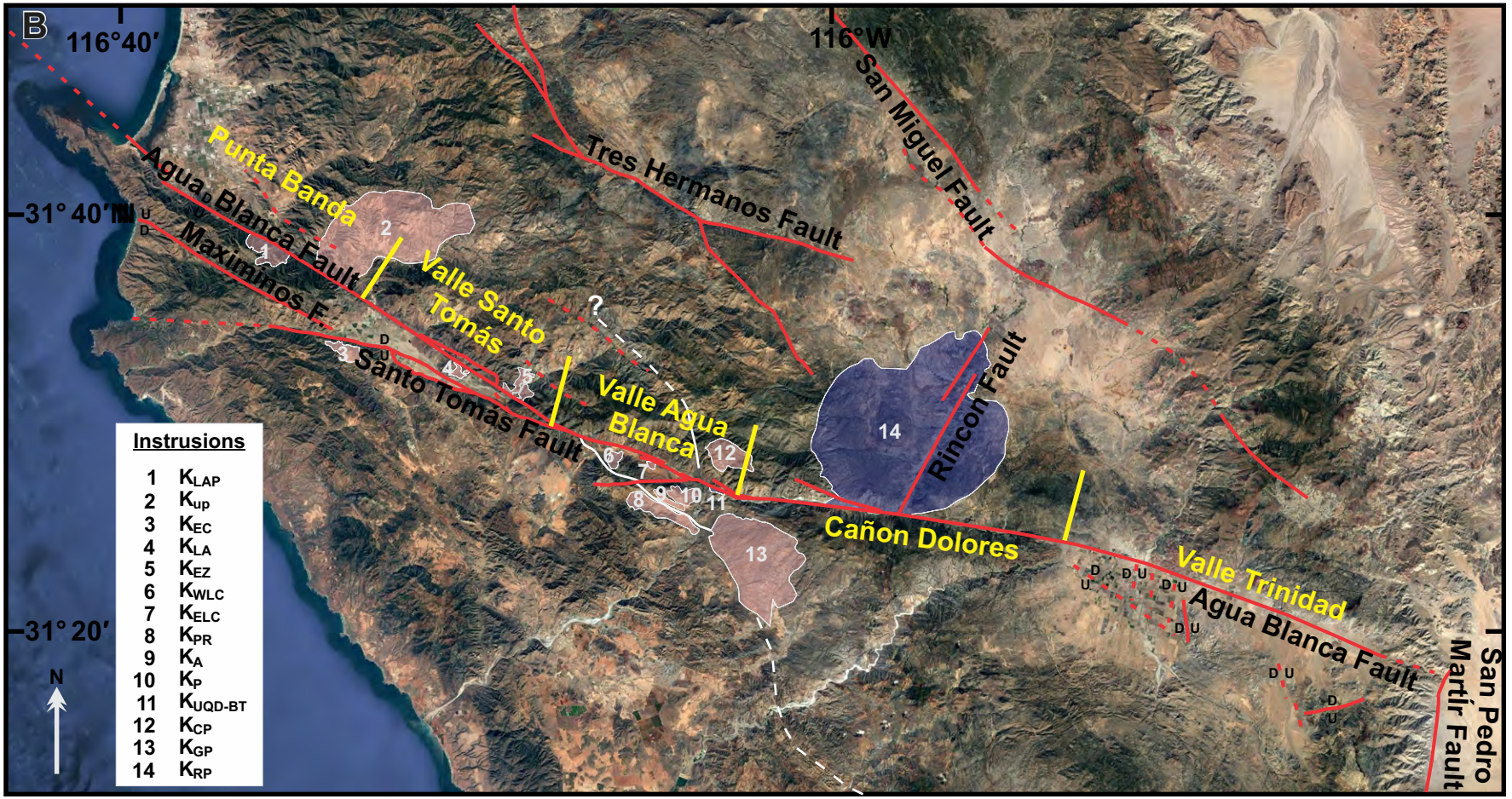

Figure 2 (*continued*). (B) Map showing the traces of the Agua Blanca and other faults of Baja California Norte, as well as intrusive bodies shown in other figures and discussed in the text. Dashed faults are inferred. Yellow lines and names are the section names and their boundaries. Inferred fault traces in Valle Trinidad area were modified from Hilinski (1988).

Geologic Setting of Northern Baja California

The ABF traverses nearly the entire width of the northern Baja Peninsula from near the San Matiás Pass on the east to the north and south sides of Punta Banda, and Punta China, where the ABF, Maximinos, and the Santo Tomás fault (STF) go offshore on the west (Figs. 2A and 2B). From east to west, the ABF cuts through rocks defining four lithostratigraphic belts including: (1) the Late Proterozoic to Permian passive margin sequences; (2) Late Triassic through Jurassic turbidites combined as part of an accretionary prism; (3) Early Cretaceous island arc and continental margin arc volcanic and volcanogenic rocks; and (4) Late Cretaceous through Paleogene submarine fan deposits (Gastil, 1993). Most of these units, except the Late Cretaceous and younger deposits along the west coast, are pervasively intruded by Late Jurassic through Late Cretaceous arc-related plutons and dikes of the Peninsular Ranges batholith

(e.g., Silver and Chappell, 1988; Walawender et al., 1990, 1991; Morton and Miller, 2014). Near the center of the Baja Peninsula, the ABF offsets a major structural feature referred to as the ancestral Agua Blanca fault, which accommodated the mid-Cretaceous collision of the Alisitos arc with the North American continental margin (Wetmore et al., 2002, 2003, 2014; Alsleben et al., 2008, 2014, Schmidt et al., 2014).

The ABF has been the subject of a relatively limited number of studies over the past several decades. These include the generation of a map of the fault trace and associated geomorphic features by Allen et al. (1960) and a series of paleoseismological investigations by Rockwell and students (Hatch, 1987; Rockwell et al., 1987, 1989, 1993; Schug, 1987; Hilinski, 1988). The results from Allen et al. (1960) include estimates of total offset between 11.3 and 22.6 km and the suggestion that the apparent time since the most recent slip events decreases, and total offsets increase, toward the western end of the ABF. Total offsets reported by Allen et al. (1960) are based on the correlation of large slivers (meter scale) of granitic rock found within the fault zone with plutonic bodies adjacent to the ABF in Valle Agua Blanca. They also reported several lines of evidence for vertical movements across the fault, including triangular facets indicating north-side-down displacement on the Santo Tomás fault in Valle Santo Tomás, south-side-down displacements at the eastern end of the ABF in Valle Trinidad, and northeast-side-down displacements at the western end of the ABF at Punta Banda. Rockwell and students report an estimate of the dextral slip rate of 6 mm/yr (Hatch, 1987; Rockwell et al., 1987, 1989, 1993), determined from studies within Valle Agua Blanca, and a second slip estimate of 2.3–4.1 mm/yr from the Punta Banda section of the fault. They also report a surface uplift rate derived from the dating of marine terraces at the west end of the Punta Banda Ridge of 0.16–0.29 mm/yr (Schug, 1987; Rockwell et al., 1989, 1993).

A geodetic network (Fig. 2A) was installed in northern Baja California in 1993 by a collaboration between the University of Miami, Centro de Investigación Científica de Educatión Superior de Ensenada (CICESE), and Jet Propulsion Laboratory (JPL) to help constrain relative motions across the ABF, San Miguel-Vallecitos fault, and other lesser transpeninsular faults in northern Baja California. Results from this network suggest that this system of faults accommodates a total motion of 4–8 mm/yr (Bennett et al., 1996; DeMets and Dixon, 1999; Dixon et al., 2002; Plattner et al., 2007; Wdowinski et al., 2007). However, details of how slip is partitioned onto each individual fault in this network remain problematic. Despite geomorphologic and paleoseismic evidence that the ABF is the most active fault in the system (e.g., Rockwell et al., 1993; Hirabayashi et al., 1996), the most recent analysis of the geodetic data using elastic models suggests that the majority of the slip is accommodated along the San Miguel–Vallecitos fault (e.g., Dixon et al., 2002; Plattner et al., 2007). Dixon et al. (2002) report a rate of 2–3 mm/yr for the ABF and 2–4 mm/yr for the San Miguel–Vallecitos fault based on elastic half-space modeling. However, they also indicate that the apparent inconsistency between the modeling and geologically inferred rates may be related to the fact that the two faults are at different stages in their respective earthquake cycles. For example, while the ABF has not had a major historical earthquake, the San Miguel–Vallecitos fault had three strong earthquakes of magnitude 6.8, 6.4, and 6.3 within one week in 1956 (Doser, 1992). Thus, by taking into account the difference in timing of their earthquake cycles, as well as incorporating a viscoelastic rheology for the upper mantle, Dixon et al. (2002) estimated a rate of 6 ± 1 mm/yr for ABF. More recently, geodetic studies in northern Baja California have been principally carried out to evaluate the effects of the 2010 Sierra El Mayor–Cucapah Mw 7.2 earthquake (e.g., Gonzalez-Ortega et al., 2014). In response to this earthquake, the Plate Boundary Observatory (PBO) continuous GPS network has been extended south of the U.S.-Mexico border with the installation of eight continuous instruments. Unfortunately, the majority of the time series of these stations are strongly affected by postseismic relaxation and, therefore, cannot be employed in this study of the long-term slip rate of the ABF.

BEDROCK GEOLOGY AND ACROSS-FAULT CORRELATIONS

One of the primary goals of this study is to extend the initial work of Allen et al. (1960) by better constraining the total displacement and sense of slip along the western two-thirds of the ABF and the Santo Tomás fault (STF), a branch of the ABF located along the southwest side of Valle Santo Tomás (Fig. 2). Therefore, the total slip of these two faults has been estimated through bedrock mapping of various Mesozoic geologic features that are cut by the active faults, including plutonic bodies, the western margin of the San Marcos dike swarm, and the ancestral Agua Blanca fault. These features have been mapped at varying degrees of detail during several trips to the region over the past 18 years. Some maps presented herein have been informed by previously published maps by Wetmore et al. (2005) (Fig. 5) and Cage (2010) and Kretzer (2010) (Fig. 7).

This study follows the traditional subdivision of the ABF into five main sections (e.g., Allen et al., 1960), defined based on changes in orientation, kinematics, and the configuration and interaction between individual fault strands (Fig. 2B). From east to west, these are Valle Trinidad, Cañon Dolores, Valle Agua Blanca, Valle Santo Tomás, and Punta Banda. The Valle Trinidad section, which was not mapped during this study, has a curvilinear trace with several prominent right-stepping bends and an average orientation of a 289°, extending ~29 km in length. This fault section controls Valle Trinidad, which is a major sedimentary basin that reaches 10 km in width (Hilinski, 1988). Although we have not yet identified offset markers across this section, its maximum finite slip may reach as high as the 10–12 km documented in the Cañon Dolores section immediately to the west (see descriptions below). However, in the Valle Trinidad section, finite slip must undergo a strong eastward-decreasing gradient as numerous fault splays extend southward into the Valle Trinidad basin from the main trace of the ABF (Fig. 2B; Hilinski, 1988). The following sections describe in detail the relevant basement geology and geomorphology in each fault section from Canon Dolores to Punta Banda.

Cañon Dolores Section

The Cañon Dolores section extends from the easternmost part of Valle Agua Blanca to the westernmost portion of Valle Trinidad (Figs. 2B and 3) and is formed by the Rio San Vicente. The main strand of the ABF appears to be located along the valley floor or following the southern edge of the Cañon through much of its length, only cutting through the bounding hills to the north at the far-western end where the fault trace exhibits a change in trend from ~276° to ~290° (Fig. 3). The geologic map was completed through air photo and satellite image analysis and reconnaissance-level mapping. The ABF in Cañon Dolores trends ~276° and cuts through various lithologies including Jurassic–Cretaceous(?) orthogneiss, the San Marcos dike swarm, the Santiago Peak

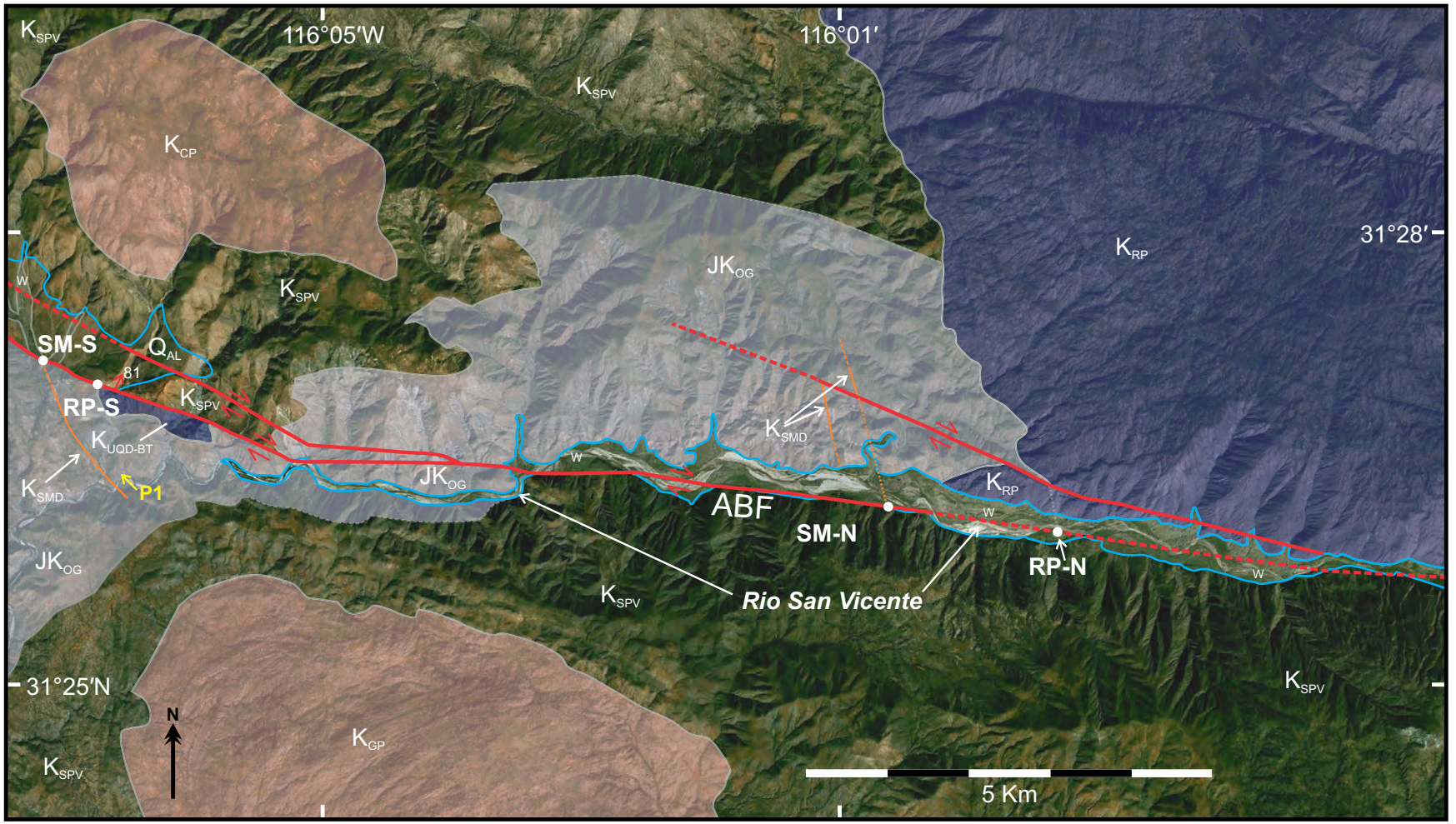

Figure 3. Geologic map of the western half of the Cañon Dolores segment of the Agua Blanca fault (ABF). Map units depicted include: K_{RP}—Rincon pluton; JK_{OG}—orthogneiss; K_{SPV}—Santiago Peak volcanics; K_{GP}—Gigante pluton; K_{CP}—Las Cuevas pluton; K_{SMD}—San Marcos dike swarm; K_{UQD-BT}—undifferentiated quartz-diorite/biotite-tonalite intrusive body; Q_{AL}—alluvial fan; and W—active fluvial wash deposits. Yellow arrow (P1) shows location and direction of photo shown in Figure 4. Projected intersections between the ABF and offset markers and/or structures include: the Rincon pluton north (RP-N) and south (RP-S) of the ABF and the western margin of the San Marcos dike swarm north (SM-N) and south (SM-S) of the ABF.

volcanics, the Rincon pluton, and late Quaternary alluvium. Two subordinate faults with subkilometer offsets branch from the ABF. Both trend northwestward away from the main fault. Offset on the westernmost fault is unconstrained but may only be a few hundred meters. The eastern fault offsets the southwestern margin of the Rincon pluton by ~0.5 km.

In the Cañon Dolores section, there are at least two bedrock units that are cut by the ABF and afford the possibility of constraining the total offset of the fault. These units are the San Marcos dike swarm, specifically its western margin, and the southwestern margin of the Rincon pluton. The San Marcos dike swarm is a regionally extensive suite of middle to late Early Cretaceous dikes (e.g., Farquharson, 2004). Strong overlap in geochemical composition and ages suggests that the dike swarm is, at least in part, associated with the plumbing system that led to the extrusion of the Santiago Peak volcanics (Wetmore et al., 2005; Herzig and Kimbrough, 2014; Schmidt et al., 2014). While the San Marcos dike swarm intrudes various lithologies, including Late Jurassic and Early Cretaceous plutons, as well as the Santiago Peak volcanics (e.g., Farquharson, 2004; Wetmore et al., 2005), it appears to be confined to the Late Jurassic–Early Cretaceous(?) orthogneiss in the Cañon Dolores area (Fig. 3). Felsic dikes, common to other portions of the swarm (Farquharson, 2004; Wetmore et al., 2005), are not observed in this area. The western margin of the dike swarm in Cañon Dolores appears to be defined by a dense cluster of mafic dikes (i.e., <2 m between dikes; Fig. 4) with no additional dikes observed farther west and a more sparse distribution to the east of the main cluster at the margin. The dikes and the western margin of the swarm strike northwest (~310°–345°) and are essentially vertical. At the western end of Cañon Dolores, south of the ABF, the dike swarm is well exposed (e.g., Figs. 3 and 4) and can be traced to within ~0.2 km of the ABF (assuming shortest distance) and ~0.5 km (if extrapolating the strike of the western margin of the dike swarm).

The western margin of the dike swarm north of the ABF is located near the center of the portion of the Cañon Dolores section depicted in Figure 3, though it is not as clearly defined here as it is to the south of the ABF. This is due to a relatively thick section (~100–200 m) of fault rocks (breccia and gouge) present along the north side of the western half of Cañon Dolores (e.g., Allen et al. [1960] mapped this as a crush zone). However, the western margin of the swarm is defined in the hills above or just outside the Cañon through field and satellite and/or air photo inspection. The total offset inferred from the margin of the dike swarm is taken as the intersection of the projection of the margin from north of the eastern subordinate fault to the trace of the main strand of the ABF, as this includes the offset of both structures. The distance between the projected intersection of the western margin of the dike swarm north and south of the ABF is 10.6 ± 0.5 km for the distance measured along the fault trace.

In addition to the San Marcos dike swarm, the Rincon pluton (K_{PR}) provides a second opportunity to constrain the total offset of the ABF in the Cañon Dolores section. The majority of the Rincon pluton is present to the north of the ABF in the central part of Cañon Dolores (Fig. 3) and is entirely within the Jurassic–Early Cretaceous(?) orthogneiss at its current level of exposure. It is a relatively coarse grained (5–10-mm-diameter crystals) intrusive body composed of biotite tonalite and subordinate dark-gray, quartz diorite phases exhibiting undeformed magmatic textures. In satellite images, the Rincon pluton appears to be a maximum of ~14 km wide in an east-west direction with well-defined host-rock contacts along the eastern and western margins. The southern margin is cut by the ABF, and the northern margin of the Rincon pluton is concealed beneath Quaternary sediments. There are only two intrusive bodies present immediately south of the ABF to the west of the Rincon pluton in the central Cañon Dolores. The westernmost of these bodies is the eastern La Cocina pluton (Fig. 5: K_{ELC}), a fine-grained (1–3-mm-diameter crystals), light-gray, hornblende quartz diorite near the center of Valle Agua Blanca. At the present level of exposure, the eastern La Cocina pluton appears to be hosted entirely within Early Cretaceous Santiago Peak volcanics. The distance along the trace of the fault separating the western margin of the Rincon and

Figure 4. Photo of an exposure of the San Marcos dike swarm located near the western end of Cañon Dolores (see Fig. 3), taken looking toward the northwest.

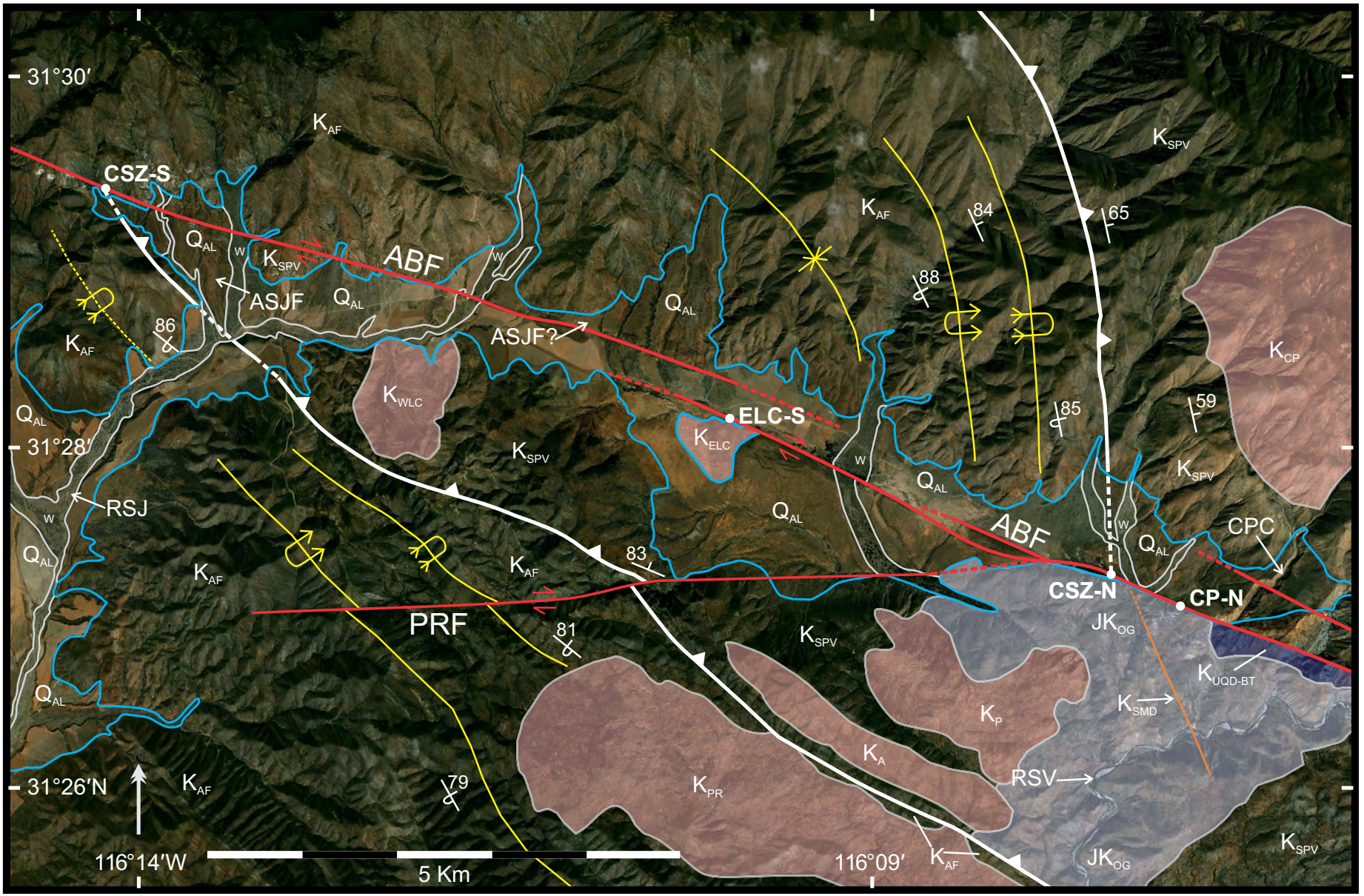

Figure 5. Geologic map of Valle Agua Blanca. Map units depicted include: JK_{OG}—orthogneiss; K_{SPV}—Santiago Peak volcanics; K_{CP}—Las Cuevas pluton; K_{P}—Pedrogoso pluton; K_{A}—Arce pluton; K_{PR}—Piedra Rodada pluton; K_{AF}—Alisitos Formation; K_{ELC}—Eastern La Cocina pluton; K_{WLC}—Western La Cocina pluton; K_{SMD}—San Marcos dike swarm; K_{UQD-BT}—undifferentiated quartz-diorite/biotite-tonalite intrusive body; Q_{AL}—alluvial fan; and W for active fluvial wash deposits. Also identified are the locations for: RSV—Rio San Vicente; CPC—Cañada Paredes Coloradas; PRF—Piedra Rodada fault; ASJF—Arroyo San Jacinto fan, Rio San Jacinto. The projected intersections between the Agua Blanca fault (ABF) and the Cretaceous shear zone north (CSZ-N) and south (CSZ-S) of the fault are also depicted.

the Eastern La Cocina plutons is ~19.0 ± 1.0 km. The other intrusion present in the southern wall of the ABF is a small unnamed (Fig. 3: $K_{UQD\text{-}BT}$) elongate body (1.4 × 0.3 km) located near the transition between Cañon Dolores and Valle Agua Blanca. It is strongly brecciated except for some exposures in the small canyons leading away from the ABF; these exposures included dark-gray quartz diorite and some coarse-grained, biotite tonalite. In addition to the similarities in lithology that $K_{UQD\text{-}BT}$ shares with the Rincon pluton, this small intrusion is hosted within the Jurassic–Early Cretaceous(?) orthogneiss and is a short distance (~0.8 km) east of the western margin of the San Marcos dike swarm, just as the Rincon pluton is to the north of the ABF. The distance along the trace of the fault separating the western margin of the Rincon pluton north of both the ABF and the subordinate splay (Fig. 3) and the western margin of the small unnamed intrusive body south of the ABF is 11.9 ± 0.2 km.

The discrepancy between the two offset measurements listed above (i.e., 10.6 ± 0.5 km and 11.9 ± 0.2 km) likely reflects the fact that the western margin of the Rincon pluton is characterized by some sinuosity in the area close to the fault (Fig. 3). For example, where the pluton margin is cut by the small-offset fault strand just north of the main strand, the trend of the margin north of this fault is northwest-southeast, whereas to the south of the subordinate fault, it trends northeast-southwest. We contend, therefore, that the measurement derived from the western margin of the San Marcos dike swarm (10.6 ± 0.5 km) is likely to be the more accurate of the two.

The kinematics of slip within the Cañon Dolores section cannot be uniquely defined due to the lack of clear piercing point but do appear to be nearly pure strike slip based on the observations that there are no clear scarps or other geomorphic indicators for a significant component of dip-slip motion. However, mismatches between the length of the Rincon Pluton along the ABF and the small unnamed intrusion ($K_{UQD\text{-}BT}$), and the distance between these intrusions and the western margin of the San Marcos dike swarm, do suggest the possibility for some amount of dip-slip displacement. However, the sense of slip is not clear. The swarm is vertical, and the contact between the host rocks and the Rincon Pluton is vertical to gently west dipping, which, given the greater distance between these two features on the north wall suggests north side down, while the average elevation of the peaks north of Cañon Dolores is ~200 m higher than those to the south. Either way, the apparent vertical component of slip on the ABF appears to be no more than a few hundred meters or less than a few percent of the total displacement on the fault in this section.

Valle Agua Blanca Section

The Valle Agua Blanca section, the type locality for the ABF (Allen et al., 1960; Silver et al., 1963), extends from the northeast corner of Valle San Jacinto on the west to Cañon Dolores on the east (Figs. 2B and 5). It is characterized by a drainage divide located between the western and eastern La Cocina intrusions (Fig. 5: K_{WLC} and K_{ELC}), with the western valley drained to the west by the Rio San Jacinto and the eastern valley that comprises several unnamed streams draining east into the Rio San Vicente (present in the southeast corner of Fig. 5).

The ABF in the Valle Agua Blanca section is well defined, exhibiting many prominent features common to strike-slip faults (e.g., pressure and shutter ridges and the vegetative effects of a perched groundwater table). The trend of the ABF in Valle Agua Blanca is ~290°. The trace of the ABF entering Valle Agua Blanca from Cañon Dolores is characterized by a small (~0.3 km) left bend forming a low (40 m) pop-up. Near the center of Valle Agua Blanca, the ABF takes an ~0.5 km right step. The expected transtensional tectonics of this releasing stepover explain the existence of the Valle Agua Blanca, which we interpret to be a narrow pull-apart basin bounded by the two misaligned fault strands (e.g., Allen et al., 1960). In addition to the ABF, a small-offset subordinate fault, reported here as the Piedra Rodada fault, has an east-west trend and a trace that projects back toward the ABF near the "pop-up" at the east end of Valle Agua Blanca. The Piedra Rodada fault appears to have a dextral shear sense based on the small offsets (<100 m) of several Early Cretaceous structures, including the ancestral Agua Blanca fault (Fig. 5).

The ancestral Agua Blanca fault was identified from detailed mapping of the bedrock geology of the Valle Agua Blanca area. It is inferred to represent a non-terminal suture formed during the mid-Cretaceous collision of the Alisitos arc with the North American continental margin (e.g., Wetmore et al., 2002, 2003, 2005, 2014; Alsleben et al., 2008, 2011, 2014; Schmidt et al., 2014). To minimize confusion created by the similarity of the names of this and the active structure, we will continue to refer to the active structure as the ABF, and we will refer to the ancestral Agua Blanca fault as the Cretaceous shear zone for the remainder of this contribution. The Cretaceous shear zone, depicted as the heavy white toothed line in Figure 5, is a northwest-trending, northeast-dipping, 100–300-m-wide mylonitic shear zone. It juxtaposes the subaqueous volcanics, volcaniclastics, and carbonates of the Alisitos arc terrane to the south, with Triassic–Jurassic turbidite sequences and intrusions (orthogneisses) overlain by the Early Cretaceous Santiago Peak volcanics and associated intrusions, which are interpreted to be the North American accretionary prism and successor arc, respectively (Wetmore et al., 2002, 2003, 2005).

The Cretaceous shear zone can be traced nearly continuously south of the ABF in the area depicted in Figure 5. Here, the Cretaceous shear zone, and associated folds, trend northwest and are well exposed in the hills along the south side of Rio San Jacinto and along the northeast side of a short northwest-trending ridge located between the stream channel and the ABF. The Cretaceous shear zone to the south can be traced to within 50 m of its intersection with the ABF. The Cretaceous shear zone and associated folds north of the ABF are located north and northeast of the central and eastern portions of Valle Agua Blanca and are characterized by north-south trends within ~2–3 km of the active ABF. Farther north, these structures exhibit a gradual change in trend toward northwesterly directions. Immediately north of the ABF, the Cretaceous shear zone is well exposed, and observable even in satellite imagery, to within ~1 km of the active structure, thus requiring extrapolation of the shear zone trend across the northern portion of the Agua Blanca (alluvial) fan (Fig. 5). The

distance along the trace of the ABF separating the two intersections of the Cretaceous shear zone with the ABF is 11.2 ± 2 km.

The kinematics of slip along the ABF in the Valle Agua Blanca section is dominated by pure strike slip as indicated by an alluvial fan cut by the active structure. At the eastern end of Valle Agua Blanca, the ABF cuts the Agua Blanca fan (as defined by Allen et al., 1960; and mapped as unit Q_7 by Hatch, 1987) and displaces the southern half of this fan to a position ~5 km to the west in the central portion of the Valle (Fig. 5). The northern half of the fan, which has been partially dissected by erosion, still maintains a well-preserved surface near Cañada Paredes Coloradas, which has an elevation at the ABF of ~500 m asl (Fig. 5). The Agua Blanca fan south of the ABF is transected by a few minor active channels but has otherwise avoided any other pronounced modification, particularly in the portion east of the eastern La Cocina pluton (Fig. 5: K_{ELC}), where the elevation of the fan surface at the ABF is ~520 m asl.

Drainage Reorganization from Valle San Jacinto to Cañon Dolores

A test of the accuracy of slip determinations derived from offset markers from the Valle Agua Blanca section is possible using the numerous drainages that cross the ABF in and around the Valle Agua Blanca. Rio San Vicente dominates the drainage in the eastern half of the area from Valle San Jacinto (just west of Valle Agua Blanca) through the western half of Cañon Dolores (Fig. 6). However, numerous smaller drainages also cross the ABF from the north along this length. The present-day drainage divide between Valle San Jacinto and Valle Agua Blanca is located between the western and eastern La Cocina plutons (K_{WLC} and K_{ELC}; Fig. 5). To the west, there are five well-defined drainages at the heads of large alluvial fans that stretch across Valle San Jacinto (~6.5 km). The catchments that these drainages and fans are currently sitting in front of have areas that range from <1 to ~7 km^2, which are much too small to have been the sources for these large fans. When 11.2 km of dextral strike-slip motion is restored, however, these five drainages line up almost perfectly with catchments that have areas that range from 8 to 24 km^2 for the four drainages within Valle Agua Blanca and >600 km^2 for the Rio San Vicente drainage basin flowing out of Cañon Dolores, which aligns with the easternmost drainage from Valle San Jacinto (Fig. 6B). While fan size is not uniquely correlated with catchment area, in this example, the source rock compositions and elevations to the north of the ABF are quite uniform, and no pronounced variations in subsidence rates have been observed between Valle San Jacinto and Valle Agua Blanca. Thus, we are confident this lends strong support to the total slip determinations derived from Cretaceous features in Valle Agua Blanca and Cañon Dolores.

Valle Santo Tomás Section

Valle Santo Tomás is a narrow, northwest-trending, elongate (~45 × 3 km) valley that is bound by the ABF on the northeast and the Santo Tomás fault (STF: following Gastil et al., 1975 and Rockwell et al., 1993), on the southwest. The trace of the ABF crosses over the pass between Valle San Jacinto and Valle Santo Tomás, entering the latter at its southeastern corner (Figs. 2B and 7). Somewhere within this pass, the ABF splits into two subparallel faults with the STF following the same approximate strike as the ABF in Valle Agua Blanca (i.e., ~290°) and the trend of the ABF being slightly more northerly at ~302°.

Agua Blanca Fault in Valle Santo Tomás

The ABF enters Valle Santo Tomás near the mouth of Cañon El Zacatón, passes through low foothills on the north side of the Cañon, and crosses a series of alluvial fans along the northeast side of the valley (Fig. 7). Approximately 2 km northwest of Cañon El Zacatón, a second fault strand breaks off from the ABF with a northerly trend for ~1 km before assuming a northwesterly trend subparallel to that of the ABF. This fault strand, referred to here as the Rancho El Roquete strand (RER), extends for ~7.6 km before recombining with the ABF near Cañon Verde (CV). In the central part of the Valle Santo Tomás section, the ABF and the RER are separated from the main part of the valley by a series of low hills. Nearly everywhere in this section, the strikes of both the ABF and RER are parallel to the strike of bedding in the Alisitos Formation (K_{AF}), a unit composed of volcanic rocks and associated epiclastic volcanic rocks deposited in a subaqueous environment (e.g., Silver et al., 1963; Allison, 1974). Therefore, the best targets for estimating the total offset of this part of the fault are the plutonic bodies cut by the fault in the eastern half of Valle Santo Tomás.

Southwest of the ABF is the Los Alisos pluton (K_{LA}, Fig. 7). Originally mapped by Kretzer (2010), it is exposed at the southeast end of the low hills separating the ABF from the central part of Valle Santo Tomás. To the north of the fault is the El Zacatón pluton (K_{EZ}), located at the mouth of Cañon El Zacatón. The northwestern margin of the Los Alisos pluton includes a subhorizontal roof and a subvertical wall that can be traced to within ~50 m of the ABF trace. The southeastern margin of the Los Alisos is concealed beneath Quaternary alluvium. The northwestern margin of the El Zacatón pluton is clearly exposed where it is cut off by the ABF in the low hills to the northwest of the mouth to Cañon El Zacatón. The distance along the trace of the ABF separating the northwestern margins of the Los Alisos and El Zacatón plutons is 4.9 ± 0.2 km.

Alternative correlations for the Las Animas and El Zacatón plutons are possible, including the Las Cuevas pluton in Valle Agua Blanca (K_{LC}, Fig. 5) and the Las Animas pluton in Valle Uruapan (K_{LAP}, Fig. 10). The Los Alisos pluton may be matched with the Las Cuevas pluton in the northern wall of the ABF at the far eastern part of Valle Agua Blanca with a separation of 25 ± 3.5 km. Similarly, an offset of the southwestern part of the El Zacatón pluton may be represented by Las Animas pluton located 27 ± 2.0 km in Valle Uruapan. While the similarity in the distances separating the Los Alisos from the Las Cuevas and the El Zacatón from the Las Animas plutons suggest the potential for the validity of the correlation of these units, they are contradicted by their distinctive petrographies. Whereas the Los Alisos and El Zacatón plutons are petrographically similar to one another, the Las Animas and the Las Cuevas plutons are

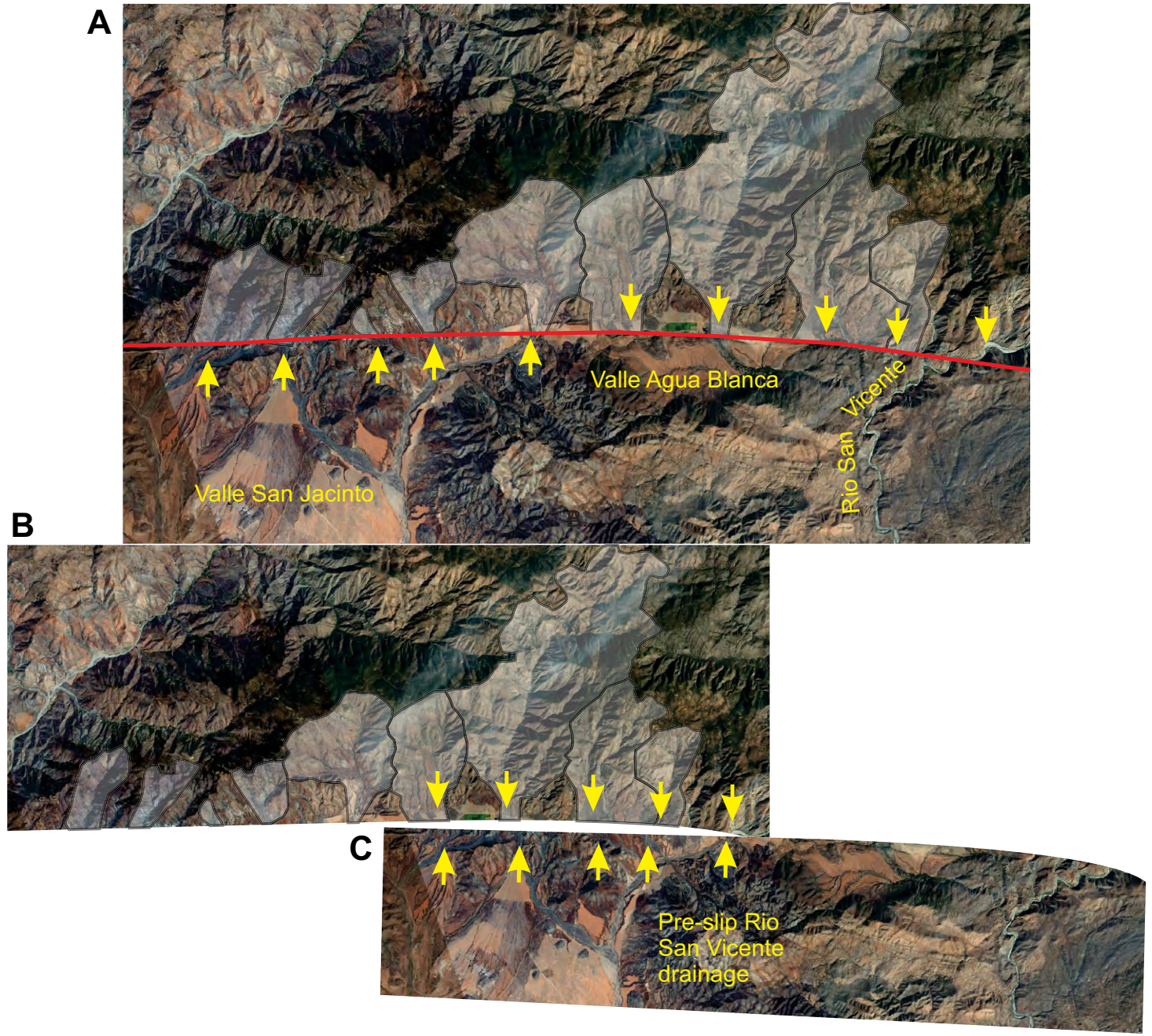

Figure 6. (A) Map of the drainage basins north of the Agua Blanca fault (ABF) in Valle Agua Blanca and Cañon Dolores. (B) Present basin and drainage configuration with yellow arrows shows the positions of the five main drainages south of the fault in Valle San Jacinto and the exits for the four main drainage basins in Valle Agua Blanca and the Rio San Vicente drainage basin at the western end of Cañon Dolores. (C) Restoration of 11.2 km of dextral strike-slip displacement showing the alignment of drainage basin exits with heads of drainages at the ABF.

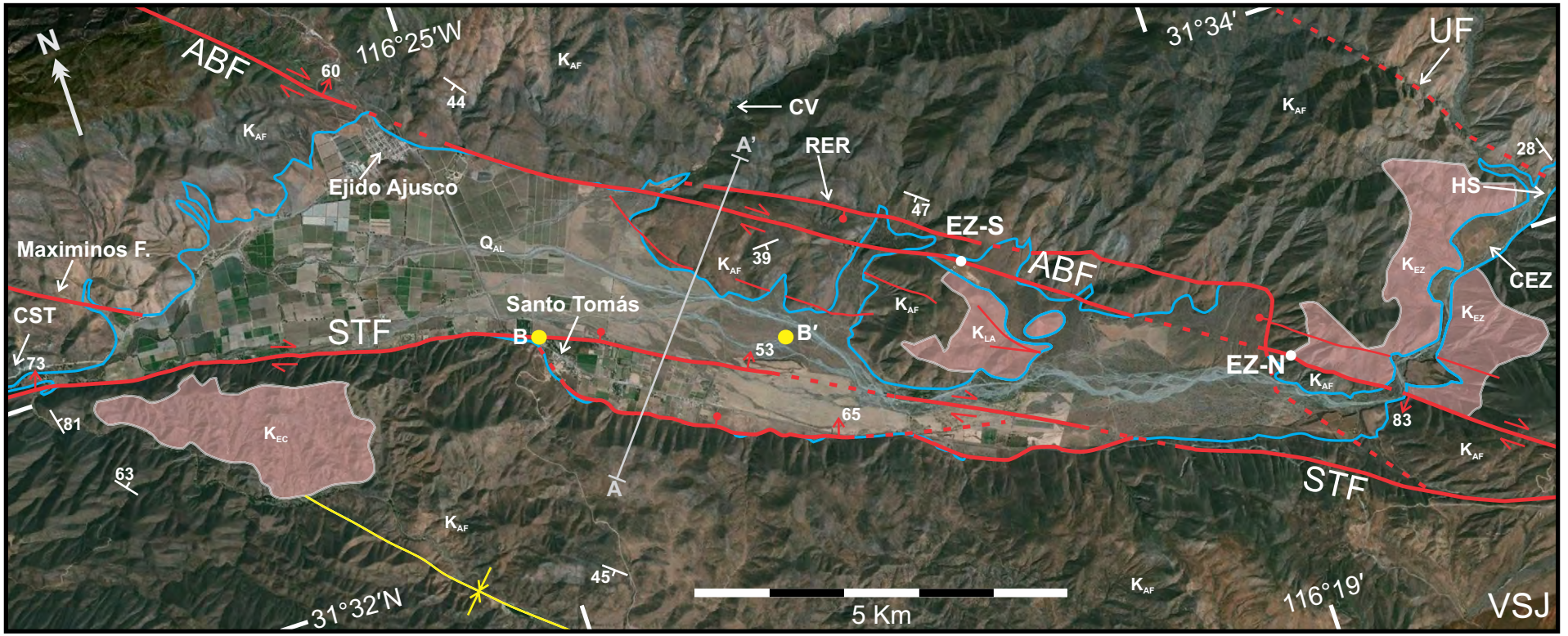

Figure 7. Geologic map of Valle Santo Tomás. Map units depicted include: K_{EZ}—El Zacatón pluton; K_{LA}—Los Alisos pluton; K_{EC}—El Chocolate pluton; K_{AF}—Alisitos Formation; Q_{AL}—alluvium; UF—unnamed fault. Also identified are the locations for: CEZ—Cañon El Zacatón; RER—Rancho El Roquete; CV—Cañon Verde; CST—Cañon Santo Tomás; and VSJ—Valle San Jacinto. The projected intersections between the Agua Blanca fault (ABF) and the northwest margin of the Los Alisos pluton (EZ-S) and the northwest margin of the El Zacatón pluton (EZ-N), as well as the location of the profile of the gravity model (A–A'), are depicted.

quite distinct from the intrusions of Valle Santo Tomás. The Los Alisos and El Zacatón plutons are composed of light-gray, fine-grained (1–2 mm plagioclase and biotite crystals) tonalites, while the Las Animas is much darker and more coarse grained (2–5 mm long biotite crystals), and the Las Cuevas is a light-gray granodiorite with distinctive quartz crystals and dark-green xenolithic inclusions that can comprise as much as 60% of the rock by volume (Allen et al., 1960). We believe, therefore, that the most likely correlation is between the Los Alisos and El Zacatón plutons indicating 4.9 ± 0.2 km of slip along the ABF in this part of the fault.

In general, the ABF in Valle Santo Tomás appears to be characterized by nearly pure strike slip. This inference is supported by the observation that along the entire length of the main strand of the ABF, surface displacements suggestive of a vertical component of slip are only observed where slip has juxtaposed different parts of a sloping surface (e.g., alluvial fan) such as is the case near point EZ-S (Fig. 7). The one exception to this is the RER fault strand, which is associated with truncated spurs where it trends toward the north at its southernmost extent and a prominent ~2-m-high scarp indicating a south-side-down component of dip-slip motion near the middle of its trace (Fig. 8). The exposure of bedrock in shallow stream beds on either side of the fault, and the results of a ground penetrating radar survey across this fault (Kretzer, 2010) reveals only a few decimeters of sediment overlying the bedrock. These observations suggest that the El Roquete strand has not accommodated much more vertical offset than the observed ~2 m in its central section. However, the total amount of dip-slip displacement at its southernmost (north-trending) part is at least ~10 m based on the heights of the truncated spurs, and perhaps as much as a few hundred meters based on the topographic difference between the fan and hills across the fault to the southeast.

Figure 8. Photographs looking northeast at the El Roquete strand of the Agua Blanca fault (ABF) in the Valle Santo Tomás section. (A) An ~2-m-tall fault scarp defined by a break in slope and clustering of larger trees on the down-dropped southwestern wall (foreground). (B) Location of the fault trace.

Santo Tomás Fault in Valle Santo Tomás

The STF in Valle Santo Tomás can be divided into three sections based on the number of strands and trends of the fault traces. The southeastern section is characterized by a single fault trace, which trends ~290° (the same as the ABF in Valle Agua Blanca) and is present along the base of the hills bounding the valley along its southwestern side. In the central part of Valle Santo Tomás, the STF splits into southern and northern strands. The trace of the southern strand continues to follow the base of the hills, and the strike of its trace is variable, including an ~354° trend where it recombines with the northern strand in the town of Santo Tomás. The northern strand traverses the central portion of the valley (Fig. 7) with a trend of ~296°. The western part of the STF is again a single fault that follows the base of the ridge and trends ~283° away from the town of Santo Tomás along the western end of Valle Santo Tomás at the head of Cañon Santo Tomás. There, the fault cuts into the hills on the north side of the Cañon. Beyond this point, the trace of the STF is difficult to identify due to the lack of clearly offset markers, dense vegetation, and an apparent decrease in the magnitude of the dip-slip motion on this part of the fault (see discussion below). Presumably, however, the STF to the west assumes a more westerly trend and passes offshore at Bahía Soladad (Allen et al., 1960; Legg, 1985; Legg et al., 1991) (Fig. 2). Additionally, another fault—the Maximinos fault—can be traced from the northern edge of Valle Santo Tomás, ~1 km northeast of the head of Cañon Santo Tomás (Fig. 7), northwestward to the Pacific coast just south of the Punta Banda ridge (Fig. 2). Thus, somewhere in the valley between Cañon Santo Tomás and the town of Santo Tomás, the Maximinos fault must branch off from the STF.

The entire length of the STF within Valle Santo Tomás, including both fault strands in its central portion, possesses surface displacements suggesting a component of northeast-side-down, normal dip-slip displacement (Allen et al., 1960; Schug, 1987). The northern strand of the central section, in particular, is characterized by a ~4-m-high scarp within the town of Santo Tomás, where it merges with the southern strand. Likewise, west of the town of Santo Tomás, the western section of the STF is characterized by evidence for recent surface rupture events with a significant dip-slip component: the scarp observed in town continues for at least another two kilometers to the west, and well-defined truncated spurs are common throughout this stretch of the fault as well. However, unlike the drainages in the central section, those in the western section commonly exhibit pronounced right deflections at the STF.

Farther to the west, near the head of Cañon Santo Tomás, the STF passes into the hills on the north side of the canyon, and there are no clear indications of a north-side-down component of dip slip as is characteristic of the STF in Valle Santo Tomás. This may reflect the fact that both the STF and the Maximinos fault cut through south-facing slopes, and normal displacements on north-dipping faults might be obscured by the fact that such offsets would be generating uphill-facing scarps in the easily erodible Late Cretaceous shales of the El Rosario Formation (e.g., Allison, 1974; Gastil et al., 1975). One possible line of evidence for normal displacement on the STF, as noted by Allen et al. (1960), is the apparent sinistral offset of the gently (5°–10°) west-dipping contact between the Early Cretaceous Alisitos Formation and the overlying Late Cretaceous Rosario Formation. They note that the contact is much higher (>600 m?) on the south side of the fault than on the north, and the strike separation is ~7.3 km. This would correspond to a dip-slip displacement between 0.7 and 1.4 km, if it is indeed a structural juxtaposition. However, as noted by Allen et al. (1960), the Late Cretaceous shoreline was highly irregular, suggesting the possibility that the juxtaposition might, at least in part, be related to the topography of the substrate across which the Rosario Formation was deposited. The estimated magnitude of the north-down dip slip is entirely consistent with the thickness of basin fill in Valle Santo Tomás (discussed below). However, offsets of more than ~200 m on the STF are not supported by bathymetric and seismic data from just off the coast at Punta Soledad (Legg et al., 1991), and the expected topographic expression of a fault with significant dip slip is not obvious along this westernmost section of the STF.

Total offset across the STF cannot be demonstrated with any degree of certainty at this time due to the lack of identified structures or other geologic features (e.g., intrusions) that may be correlated across the fault. However, the maximum magnitude of total dip-slip displacement on the STF may be estimated by the results of a recent gravity survey of the Santo Tomás region (Springer, 2010) combined with the assumption that Valle Santo Tomás formed through the strike-slip and dip-slip displacements on the STF and ABF. Modeling of gravity data collected by Springer (2010) suggests that basin fill on the southwest side of Valle Santo Tomás is, in the central portion of the STF, ~400 m adjacent to the southern strand and ~800 m adjacent to the northern strand. Assuming a fault dip of ~65° to the northeast for the southern strand and 53° for the northern strand (both from field measurements; Fig. 7), plus an additional 200 m, which is the change in elevation from the valley floor to the top of the plateau to the southwest of the valley, the total dip-slip displacement on the southern strand of the STF is ~660 m with an additional ~500 m on the northern strand, for a total of ~1160 m of dip-slip offset on the central portion of the STF (Fig. 9). The corresponding heave on these faults would be ~580 m NE-SW and a total throw of 997 m. We note that since these numbers measured from the extrapolated elevation of the plateau to the southwest of the STF, they should be taken to be maximum displacements.

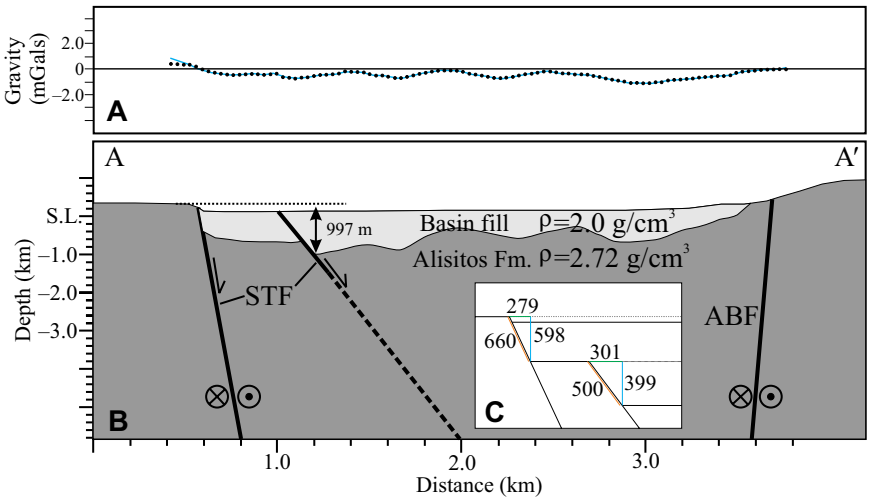

Figure 9. (A) Gravity profile. (B) Two-dimensional gravity model for the line A–A′ shown on Figure 7. Modified from Springer (2010). (C) Simplified structural breakdown showing total dip slip (orange), heave, (green), and throw (blue). ABF—Agua Blanca fault; STF—Santo Tomás fault; S.L.—sea level.

Punta Banda Section: Valle Uruapan to Las Animas

Northwest of Valle Santo Tomás, the ABF enters the Punta Banda section, where it crosses Mexican Highway 1 at the pass between this valley and the area we here refer to as Valle Uruapan (Figs. 2B and 10). Valle Uruapan includes Cañon La Grulla, where Ejido Uruapan is located, and Cañon Las Animas, which connects La Grulla with Valle Maneadero and Bahia Todos Santos (Fig. 2A). The ABF follows the base of the Punta Banda Ridge on its northeastern side from just northwest of Valle Santo Tomás to Bahia Todos Santos, where it goes offshore and becomes part of the Continental Borderlands system of faults (e.g., Legg et al., 1991). This section of the ABF, referred to as the Punta Banda segment by Rockwell et al. (1993), has been the subject of a handful of recent studies (e.g., Hatch, 1987; Rockwell et al., 1993; Madsen, 2009; Callihan, 2010), all of which have focused on the western half of the fault in Valle Maneadero.

The ABF continues to cut through the Early Cretaceous Alisitos Formation throughout the Punta Banda segment (Fig. 10). Approximately 2.5 km northwest of where the ABF crosses Mexican Highway 1, the fault cuts the southwestern end of the Uruapan pluton (K_{UP}), a late Early Cretaceous intrusion of the Alisitos Arc (Gastil et al., 1975; Wetmore et al., 2014). The Uruapan pluton is a large intrusion (>80 km^2) with steeply, outwardly dipping contacts (~70°) that appear to truncate bedding and structures in the hosting Alisitos Formation without deflection away from their regional (NW-SE) trends. The long axis of the intrusion trends northeasterly, nearly normal to that of the structural grain of the bedrock, extending more than 8 km from the ABF. The host-rock contacts of the Uruapan pluton are easily traced most of the way around the intrusion, including the point where it is cut by the ABF on the southeast side of the intrusion (i.e., UP-NE in Fig. 10). However, on the northwest side, the margin is concealed beneath Quaternary alluvium and must be projected from ~1.1 km away to its inferred intersection with the ABF (i.e., UP-NW). Based on this projection, the Uruapan pluton has a diameter of ~3.2 km along the trace of the ABF. The Uruapan pluton is a biotite tonalite with 2–5-mm-long, subhedral biotite and plagioclase feldspar crystals that typically exhibit a weak magmatic fabric. However, there are local examples of moderately strong magmatic to high-temperature subsolidus fabrics (e.g., along the southeastern margin). Also present within this intrusion are large (20–50-cm-long) microgranitoid mafic enclaves (<1%–2% of most exposures), rarely observed schlieren, and rare, large (1–2-cm-long) plagioclase feldspar crystals.

The only intrusive body identified in the southwestern wall of the ABF in the Punta Banda Ridge segment is located ~3 km to the northwest and is here referred to as the Las Animas pluton (K_{LAP}, Fig. 10). The Las Animas pluton has petrographic characteristics (i.e., modal mineralogy, grain size, fabric variations, and xenolith sizes and concentrations) and host-rock contact relationships that are essentially the same as those observed within the Uruapan pluton. The diameter of the Las Animas pluton along the ABF is ~4.0 km. If the Las Animas pluton is the displaced southwestern continuation to the Uruapan pluton, then the strike separation between the intersection of northwestern margins of these intrusions and the ABF (i.e., UP-NW and UP-SW) is 7.1 ± 2.5 km and 6.3 ± 0.3 km for the intersections of the eastern margins and the ABF (i.e., UP-NE and UP-SE). Based on the possibility of some component of dip-slip displacement (discussed below), we believe that the most accurate measurement is the separation of the middle point of each intrusion along the fault trace, and that measurement gives a displacement of 6.8 ± 2.8 km.

Observations of the offset Uruapan–Las Animas plutons suggest the potential for a component of dip-slip motion on the ABF in the Punta Banda section. The mismatch of the along-fault diameters of the two intrusive bodies (3.2 km Uruapan and ~4 km Las Animas), combined with the observation that contacts of these intrusions dip steeply outward, suggests that the northeast wall may have dropped down relative to the southwest wall. Given the ~70° outward dips of the intrusive contacts on both the north and south sides of the Uruapan pluton, the 800 m difference in the intrusive diameters along the fault, and a fault dip of 60° north (measured at the pass between Valle Santo Tomás Valle Uruapan; Fig. 7), we estimate ~1.1 km of throw, ~0.65 km of heave, and a maximum total normal displacement of 1.25 km to the north across the ABF in this section.

GPS GEODESY

The Northern Baja California geodetic network consist of 18 campaign GPS (eGPS) stations and 11 continuous GPS stations (cGPS), eight of which were installed after the 2010 El Mayor–Cucapah earthquake and are not used in this paper (Fig. 11). The 18 campaign GPS stations consist of monuments with 10-in-long stainless-steel rods epoxied into bedrock. The monuments were occupied periodically, annually or biannually, until 2001 (see Table 1). Every site utilized in this paper was occupied during at least three campaigns, with at least two full (Coordinated Universal Time) days of occupation (typically three or more) for each campaign. University of Southern Florida, working in collaboration with the University of Southern California, reoccupied the full network in 2012 and 2013. All the sites north of the LOSA station (Fig. 11) are likely to be affected by the Mw 7.2 2010 El Mayor–Cucapah earthquake. This paper does not include the newest observations from the campaign stations in the northern part of the network because they are not suitable to compute long-term interseismic velocities. Campaign data for sites south of ABF were utilized to improve the Rigid Baja reference frame. After the 2010 earthquake, multiple permanent sites were installed in the framework of the Plate Boundary Observatory (stations starting with P and ending with X; Fig. 11 and Table 1). Apart from station PSTX, all the other stations present a strong postseismic signal. The transient postseismic signal is not significant for data collected after 2013; thus, the velocities estimated for the PBO sites in this paper are limited to the time series from January 2013–June 2016. The limited length of the time series is reflected in larger uncertainties.

The raw GPS RINEX files were processed using Jet Propulsion Laboratory (JPL) code GIPSY-OASIS 6.4. For each site, we produce a daily solution estimating fiducial free position by employing a precise point positioning (PPP) strategy (Zumberge et al., 1997). Phase ambiguity resolution was performed using the single-receiver algorithm described by Bertiger et al. (2010). Application of the FES2004 ocean-loading corrections is compatible with the JPL orbits

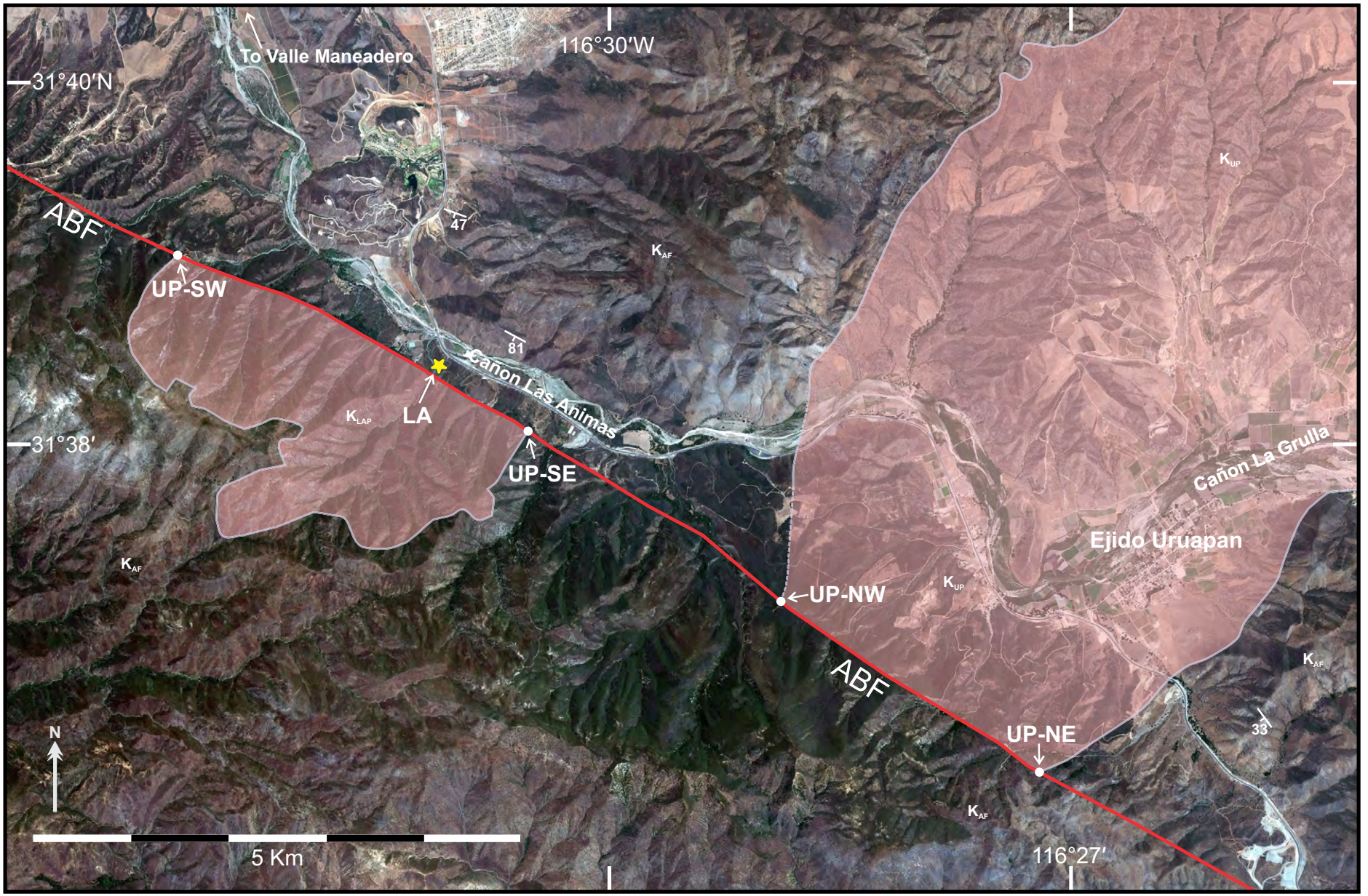

Figure 10. Geologic map of the Valle Uruapan area. Map units depicted include: K_{UP}—Uruapan pluton; K_{LAP}—Las Animas pluton; and K_{AF}—Alisitos Formation. The projected intersections between the Agua Blanca fault (ABF) and the northwest and southeastern margins of the Las Animas pluton (UP-SW and UP-SE) and the northwest and southeastern margins of the Uruapan pluton (UP-NW and UP-NE), as well as the location of the Las Animas Ranch site (yellow star labeled LA), are depicted.

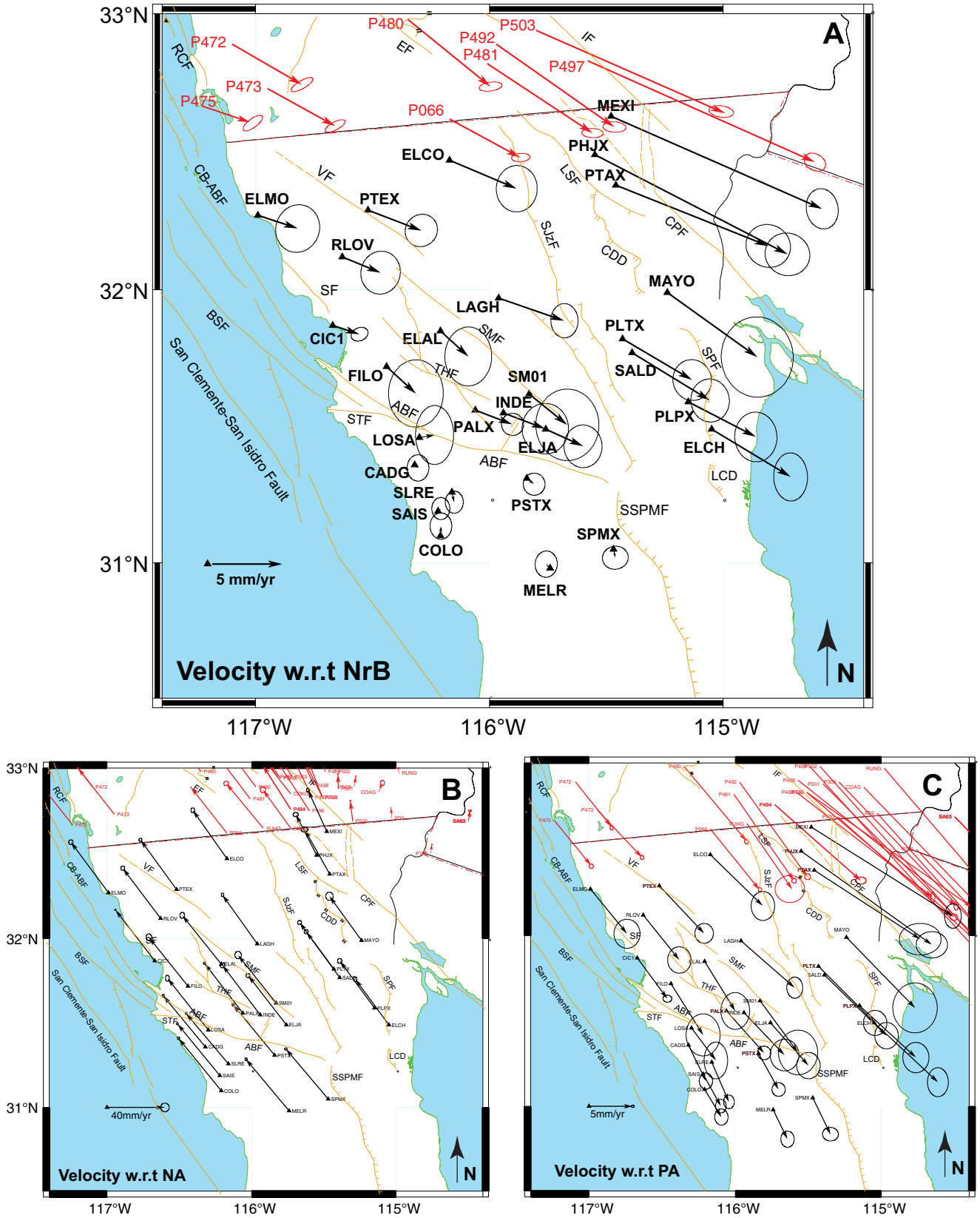

Figure 11. (A) Velocity field with respect to (w.r.t.) a rigid Northern Baja reference frame (NrB) (in black, data analyzed for this paper; in red, Plate Boundary Observatory [PBO] velocity field [Herring et al., 2016]). The velocities increase moving eastward across each fault system. The combined Agua Blanca and San Miguel–Vallecitos fault systems (transect between the stations SAIS and ELCO) accommodate ~6–7 mm/yr of relative motion. The direction of the vectors north of Agua Blanca fault (ABF) are subparallel to the fault itself, indicating that the relative motion between NrB and the Ensenada block is mainly transcurrent. (B) Velocity field with respect to a rigid fixed Pacific plate (Plattner et al., 2015). The residuals of NrB with respect to Pacific plate confirm the finding of Plattner et al. (2007) of ~5–6 mm/yr of motion of the Baja Peninsula with respect to a rigid Pacific plate (PA). (C) Velocity field with respect to rigid fixed North America (Kremer et al., 2018). Note the change of scale for this velocity field. The northwestward motion of the Baja peninsula and the blocks north of the ABF accommodate the opening of the Gulf of California. It is not possible to observe the relative motion between the different blocks in Northern Baja California at this scale.

TABLE 1. NORTHERN BAJA GEODETIC GPS NETWORK

			Velocity with respect to ITRF08									
	Position		North component			East component			Occupations history			
Station	Latitude (°N)	Longitude (°W)	Velocity (mm/yr)	WRMS (mm)	χ^2 reduced	Velocity (mm/yr)	WRMS (mm)	χ^2 reduced	First	Last	No. of campaigns	Days of observations
CADG[1]	31.36	–116.32	21.3 ± 0.6[2]	2.9	1.6	–42.9 ± 0.5[2]	2.9	1.8	1993	2012	6	26
cic1[4]	31.87	–116.67	20.9 ± 0.2[3]	0.9	0.7	–41.05 ± 0.3[3]	1.0	0.8	1999	2009	CGPS	3441
COLO[1]	31.1	–116.21	22.2 ± 0.6[2]	2.8	1.4	–43.2 ± 0.5[2]	3.0	1.9	1993	2012	8	34
elal	31.85	–116.21	19.7 ± 1.4[2]	2.3	0.9	–40.9 ± 1.1[2]	2.1	0.9	1993	2012[5,7]	6(4)[6]	30(21)[6]
elch	31.49	–115.05	18.1 ± 1.1[2]	3.2	1.5	–37.2 ± 0.8[2]	3.5	1.9	1993	2001	4	12
elco	32.47	–116.17	19.5 ± 1.1[2]	3.3	1.3	–37.8 ± 0.9[2]	3.1	1.3	1993	2012[5]	6(5)[6]	23(18)[6]
elja	31.49	–115.76	20.3 ± 1.0[2]	2.5	0.9	–40.3 ± 0.9[2]	2.4	1.1	1993	2013[5]	8(6)[6]	28(18)[6]
elmo	32.27	–116.99	20.6 ± 1.1[2]	2.8	1.2	–40.0 ± 1.0[2]	2.7	1.5	1993	2013[5]	7(5)[6]	26(18)[6]
filo	31.72	–116.44	19.6 ± 1.6[2]	3.0	1.1	–40.9 ± 1.3[2]	1.6	0.8	1993	2012[5,7]	6(4)[6]	20(11)[6]
inde	31.55	–115.94	20.4 ± 1.2[2]	3.1	1.7	–40.0 ± 1.1[2]	3.0	1.8	1993	2013[5]	7(5)[6]	32(20)[6]
lagh	31.97	–115.96	19.9 ± 0.8[2]	3.1	1.5	–38.1 ± 0.6[2]	2.4	1.1	1993	2012[5]	7(6)[6]	28(22)[6]
losa	31.46	–116.3	21.7 ± 1.4[2]	5.0	2.1	–42.0 ± 0.9[2]	2.1	0.9	1993	2013[5]	7(5)[6]	25(16)[6]
mayo	31.99	–115.24	16.9 ± 1.9[2]	3.7	1.2	–36.2 ± 1.7[2]	3.1	2.2	1995	2001	4	8
MELR[1]	30.98	–115.74	21.8 ± 0.6[2]	3.6	2.0	–43.5 ± 0.5[2]	2.3	1.9	1993	2013	6	28
mexi[4]	32.63	–115.48	14.9 ± 0.9[3]	1.4	1.2	–27.3 ± 0.6[3]	1.1	1.1	2003	2013[5]	CGPS	2988(1638)[6]
rlov	32.12	–116.63	20.4 ± 1.0[2]	3.1	1.6	–40.1 ± 0.9[2]	3.2	1.9	1993	2001	6	28
SAIS[1]	31.19	–116.22	21.7 ± 0.5[2]	3.0	1.7	–43.0 ± 0.4[2]	2.7	1.8	1993	2012	7	26
sald	31.77	–115.39	18.1 ± 1.0[2]	3.9	2.9	–37.2 ± 0.9[2]	3.2	2.1	1993	2001	4	16
SLRE[1]	31.26	–116.16	20.8 ± 0.5[2]	3.2	1.9	–43.0 ± 0.4[2]	2.9	1.7	1993	2013	13	53
sm01	31.62	–115.83	19.3 ± 1.7[2]	2.1	0.8	–40.2 ± 1.5[2]	1.0	0.7	1993	2012[5]	4(3)[6]	11(8)[6]
spmx[4]	31.05	–115.47	20.9 ± 0.5[2]	1.6	1.2	–43.0 ± 0.6[2]	1.7	1.4	1999	2011	CGPS	2412(1758)[8]
VIEJ[1]	29.08	–114.04	21.4 ± 1.4[2]	0.8	0.3	–43.5 ± 1.2[2]	1.4	0.5	2004	2012[9]	8(3)[6]	43(14)[6]
PSTX[1,4]	31.31	–115.84	21.1 ± 0.5[3]	1.1	1.0	–42.6 ± 0.5[3]	1.2	1.2	2010.6	2016	CGPS	1989(1970)[8]
ptex[4]	32.29	–116.52	20.1 ± 0.7[3]	1.7	1.3	–38.9 ± 0.7[3]	2.1	1.4	2011.3	2016	CGPS	1699(1676)[8]
palx[4]	31.56	–116.07	20.5 ± 0.5[3]	1.1	1.0	–40.4 ± 0.5[3]	2.1	1.4	2010.6	2016	CGPS	2727(2713)[8]
pltx[4]	31.82	–115.43	18.6 ± 0.9[3]	1.3	1.2	–37.8 ± 0.9[3]	2.3	1.5	2010.8[10]	2016	CGPS	1787(802)[8,10]
plpx[4]	31.59	–115.15	19.0 ± 1.1[3]	1.2	1.1	–38.0 ± 1.0[3]	1.5	1.2	2010.8[10]	2016	CGPS	2372(737)[8,10]
ptax[4]	32.37	–115.46	17.2 ± 1.2[3]	1.4	1.1	–31.6 ± 1.6[3]	4.0	1.9	2011.3[10]	2016	CGPS	1679(876)[8,10]
phjx[4]	32.49	–115.55	14.4 ± 1.0[3]	1.1	1.0	–28.7 ± 1.2[3]	2.5	1.6	2011.8[10]	2016	CGPS	1908(936)[8,10]

[1]The stations in uppercase are utilized to compute the stable Northern Baja (NrB) reference frame.
[2]Velocity uncertainties computed using Mao et al. (1998) and Dixon et al. (2000) methods.
[3]Velocity uncertainties computed using Hackel et al. (2011, 2013) (using a combination of white and powerlaw error method).
[4]Continuously operating site.
[5]Only data before 2010 El Mayor–Cucapah earthquake were used since the velocity is strongly affected by the event.
[6]In parentheses, the true number used for the analysis.
[7]Only data up to 1998 were used due to a problem in the antenna used in the 2001 campaign.
[8]In parentheses, the true number used for the analysis (many days with large uncertainties were not used).
[9]Only data until June 2009 were used since the velocity is strongly affected by a seismic event.
[10]Only data since 2013 were used since the velocity is strongly affected by a seismic event.
Abbreviations: WRMS—weighted root mean square; CGPS—continuously operated GPS station.
Note: Alternative names for the station: SLRE = LLCO, LAGH = RAYO.

calculation. Tropospheric delay is accounted for through VMF1 mapping functions. Second-order ionosphere corrections were done using the IONEX model (ftp://cddis.gsfc.nasa.gov/pub/gps/products/ionex/; Bassiri and Hajj, 1993; Kedar et al., 2003). The daily solutions were then transformed into the IGSb08 No Net Rotation reference frame (Rebischung et al., 2012) through a seven-parameters transformation using the value provided by JPL (x-files). Interseismic velocities were computed through a linear interpolation (allowing for annual and semi-annual signal) of the time series for each site and component, independently. Uncertainties for the velocity for each campaign GPS site were computed following Mao et al. (1999) and Dixon et al. (2000). For continuous sites, the velocity

uncertainties were evaluated using Hackl et al. (2011, 2013) Allan variance of the rate assuming colored noise described by white plus power law. The new analysis substantially reduces the fit weighted root mean square with respect to the previously published velocity field (i.e., Dixon et al., 2002; Plattner et al., 2007; Plattner et al., 2015) and significantly improves the uncertainties of the velocities. It is relevant to note that with this reanalysis of the data, for the first time, the velocities of the northernmost sites are perfectly compatible with the PBO-derived velocity field north of the United States–Mexico border (version 1.1.0 Release 20151223142850; Herring et al., 2016). In particular, the velocity of ELMO is equivalent to P475, ELCO to P066, and MEXI to P503.

During the 2001 campaign, the antenna used at PHYLLO and ELAL did not work properly. For this reason, the two sites have significantly shorter time series than the others, and the corresponding uncertainties are significantly larger (see Table 1).

Using the strategy described by Plattner et al. (2007, 2015) and Malservisi et al. (2013), we developed a stable Baja reference frame looking for the Euler vector that best describes the motion of the sites south of the ABF. Since we are mainly interested in the relative motion along the ABF, and we seek to avoid the problem of potential non-rigid behavior for the full Baja California peninsula reference frame as indicated by Plattner et al. (2007), we chose not to utilize the sites in the southern region of the peninsula. To avoid the large uncertainties that would be associated with the small aperture of the GPS network utilized for the Euler vector calculation, we decided to include the site VIEJ located in central Baja California (approximately at the latitude of the junction of Mexican Highway 1 with the road to Bahia de Los Angeles, ~29°N). The six sites utilized for the Euler vector calculation are indicated in capital letters in Table 1. The Euler vector that minimizes the residuals of the observed velocities of the selected sites describes the Northern Rigid Baja reference frame (NrB) with respect to the IGSb08 reference frame (Table 2). The average residual is 0.34 mm/yr, well within the average uncertainties of the used sites (0.65 mm/yr). The very low reduced χ^2 (0.4) associated with the Euler vector inversion suggests that the Mao et al. (1999) method overestimates the real uncertainties, as already noted by Hackl et al. (2011). The sites LOSA and SPMX were not included in the northern rigid Baja reference frame realization, since they are too close to the faults and are possibly affected by strain accumulation. Site PSTX does not seem to have significant influence in the minimization of the residuals having a residual well within the uncertainties whether it is used or not. Residuals, with respect to the motion described by the computed Euler vector, represent the motion of each site with respect to the NrB reference (Fig. 11A and Table 3). In other words, the residuals describe the motion of each site with respect to a fixed southern side of the Agua Blanca fault. For a better understanding of the velocity field, Figure 12 also presents the observed velocity field with respect to a fixed rigid Pacific plate (Plattner et al., 2015; Fig. 12C), and with respect to a fixed rigid North American plate (Kremer et al., 2018). Table 3 lists the Euler poles utilized for the figures.

On average, the geodetic data show that the full Baja California peninsula is translating in a northwest direction with respect to a fixed North America, in a direction compatible with the opening of the Gulf of California. With respect to NrB, we observe vectors north of the ABF oriented subparallel to the central portion of the fault. We also observe a gradient of increasing velocity from south of ABF toward the northeast. South of the ABF, the direction of the residuals for LOSA and SPMX subparallel to the trace of the ABF confirms that the interseismic velocities of these two sites are affected by strain accumulation. In the domain between the ABF and the San Miguel–Vallecitos faults, what we designate as the Ensenada block (Fig. 12), the sites ELMO, RLOV, INDE, ELJA, SM01, PALX, and CIC1 are very consistent in magnitude (average: 3.25 ± 0.3 mm/yr) and direction (average: 118 ± 6 °E), and in general are parallel to the strike of the central part of the ABF (i.e., Valle Agua Blanca through Cañon Dolores). Despite the larger uncertainties, it is interesting to note that both PHYLLO and ELAL are compatible with the velocities of the other sites within the Ensenada block. The station in Ensenada (CIC1) appears to move a bit slower than the sites just north of it, and it is probably influenced by the strain accumulation related to the change of strike of the ABF. Between the San Miguel–Vallecitos and the Sierra Juarez (SJzF) faults, here designated the Tecate block, the velocities increase to 5.6 mm/yr for sites LAGH, PTEX, and ELCO. The velocities increase further to ~6.5–7 mm/yr between SJzF, in the San Felipe block, and the main plate boundary (sites ELCH, SALD, PLPX, PLTX, and MAYO). The velocities continue to increase toward the east (PTAX, PHJX, and MEXI). These rates appear to confirm the results of Dixon et al. (2002) of ~7 mm/yr across the Agua Blanca and San Miguel–Vallecitos fault system. Postseismic relaxation appears to continue to affect the sites closest to the 2010 El Mayor–Cucapah rupture sites (PHJX, MEXI, and PTAX). To be sure not

TABLE 2. BEST-FIT EULER VECTORS FOR NORTHERN BAJA CALIFORNIA

	Ω_x (μrad/m.y.)	Ω_y (μrad/m.y.)	Ω_z (μrad/m.y.)	σ_{xx} (μrad²/m.y.)	σ_{xy} (μrad²/m.y.)	σ_{xz} (μrad²/m.y.)	σ_{yy} (μrad²/m.y.)	σ_{yz} (μrad²/m.y.)	σ_{zz} (μrad²/m.y.)
IGS08-NrB	–2.960702	1.6313577	–8.0036004	1.0966839	2.2395562	–1.5058316	4.5773682	–3.0772167	2.0694736
IGS08-PA*	–1.895492	5.1583402	–10.52478	0.0006156	0.0000309	–4.17E-05	0.000126	0.0000046	0.0001712
NrB-PA	1.06521	3.5269825	–2.521178						
IGS08-NA+	0.2426	–4.4976	–0.1396						

*From Plattner et al. (2015).
+From Kremer et al. (2018).

TABLE 3. VELOCITY FIELD WITH RESPECT TO THE RIGID NORTHERN BAJA CALIFORNIA BLOCK

	East Component		North Component		Velocity Factor	
Stations[1]	Velocity (mm/yr)	Standard deviation (mm/yr)	Velocity (mm/yr)	Standard deviation (mm/yr)	Rate (mm/yr)	Azimuth[2]
CADG	0.2	–0.3	0.6	0.5	0.4	138.4
COLO	0.0	0.3	0.6	0.5	0.3	6.7
MELR	–0.3	0.2	0.6	0.5	0.4	–50.4
PSTX	0.5	–0.4	0.3	0.4	0.6	128.7
SAIS	0.2	0.1	0.5	0.4	0.2	55.0
SLRE	0.2	–0.4	0.5	0.4	0.4	156.0
VIEJ	0.3	–0.1	1.4	1.2	0.3	110.8
elal	2.5	–1.7	1.4	1.1	3.0	123.8
elch	5.6	–3.4	1.1	0.8	6.6	121.4
elco	4.4	–3.7	1.1	0.9	5.7	130.0
elja	2.7	–1.3	1.0	0.9	3.0	115.3
elmo	2.9	–2.0	1.1	1.0	3.5	124.0
filo	2.4	–1.8	1.6	1.3	2.9	127.0
inde	3.0	–1.2	1.2	1.1	3.2	111.3
lagh	4.9	–2.5	0.8	0.6	5.5	116.8
losa	1.1	–0.3	1.4	0.9	1.1	106.8
mayo	6.4	–4.6	1.9	1.7	7.9	125.9
rlov	2.7	–1.2	1.0	0.9	3.0	113.2
sald	5.6	–3.5	1.0	0.9	6.5	121.8
sfai	2.3	–3.5	0.5	0.5	4.2	147.5
sm01	2.7	–2.3	1.7	1.5	3.5	129.7
cic1	2.4	–1.0	0.3	0.2	2.6	112.5
spmx	1.1	–0.6	0.6	0.5	1.3	116.2
mexi	15.0	–6.7	0.7	0.7	16.4	113.9
ptex	3.8	–1.5	0.8	0.7	4.1	111.0
palx	2.7	–1.0	0.5	0.5	2.8	110.9
pltx	5.0	–2.9	1.0	0.9	5.7	120.5
plpx	4.8	–2.5	1.2	1.0	5.4	117.3
ptax	10.9	–4.3	1.1	1.0	11.7	111.7
phjx	13.7	–7.1	1.1	1.0	15.5	117.3
p492	6.8	–5.9	0.3	0.3	9.0	131.0
p480	4.9	–6.2	0.2	0.2	7.8	141.8
p481	6.4	–5.8	0.3	0.3	8.7	132.3
p472	3.9	–4.0	0.2	0.2	5.6	135.7
p473	3.6	–3.7	0.2	0.2	5.2	135.8
p066	4.0	–3.9	0.2	0.2	5.6	134.5
p475	3.0	–2.2	0.3	0.3	3.7	126.2
p474	5.0	–4.6	0.2	0.2	6.8	132.7
p503	14.3	–8.5	0.6	0.3	16.6	120.7
p476	6.4	–5.9	0.2	0.2	8.7	132.6

[1]Stations in uppercase are utilized to compute the stable Northern Baja (NrB) reference frame. The middle group is made up of episodic GPS stations. The lower group is made up of continuously operated GPS stations.
[2]Azimuth from North clockwise.

to bias our interpretation due to the faster velocities of these three sites, in the following analysis, we use only data prior to the 2010 earthquake for the site MEXI, and we do not use the two PBO sites PHJX and PTAX. In general, we observe significant increases in velocity when passing across each fault in the system. However, the directions of the velocity for stations north of the ABF do not change significantly moving from west to east until we reach the main plate boundary. An analysis of the velocity field with respect to a fixed Pacific plate (Fig. 11C) confirms the finding of Plattner et al. (2007) of a motion of 6–7 mm/yr to the southeast of NrB, with a direction subparallel to the strike of the west coast of Baja California. Below we present the results of block modeling of the geodetic data to determine slip rates and along-strike changes in the character of deformation across the ABF.

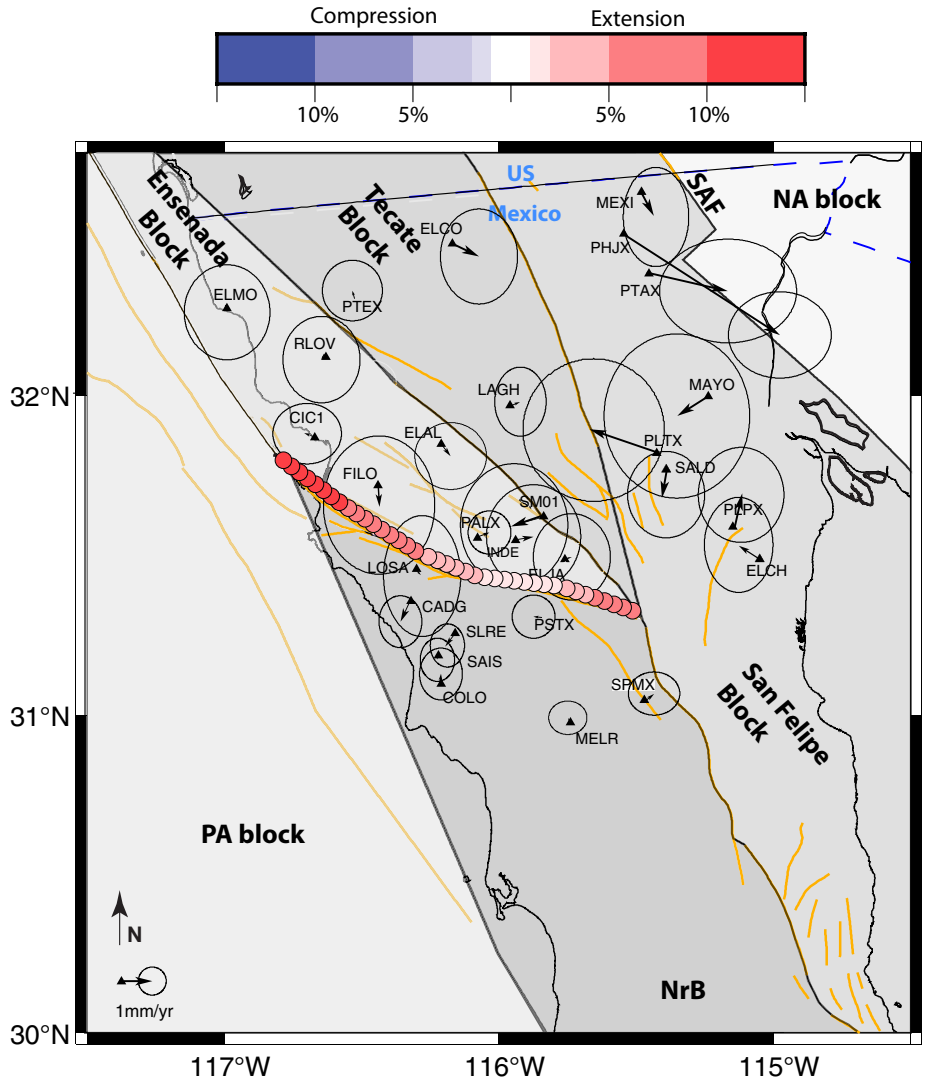

Figure 12. Residuals with respect to the six tectonic blocks defined for the rigid block rotation calculated using DEFNODE. The colored dots represent the relative amount of dip-slip motion with respect to the full computed slip rate at the block boundary. Note the larger amount of extensive dip slip required to accommodate the motion of the Ensenada block with respect to NrB moving northward. Although the partitioning between the eastern and western boundary of the Ensenada block (i.e., Agua Blanca fault [ABF] and San Miguel–Vallecitos fault) can be affected by the rheological model assumed for the calculation and the relative stage of the earthquake cycle, the partitioning between dip-slip and strike-slip motion for each fault is not significantly influenced. The large residuals of the Plate Boundary Observatory sites within the Sierra Juarez block suggest that postseismic deformation is still present also in the data observed after 2013. SAF—San Andreas fault; NA—North America; PA—Pacific plate.

Block Modeling

In order to analyze the effect of the change in orientation of the ABF on the observed velocity field, we model the data using the code DEFNODE (McCaffrey, 2002). DEFNODE is a block model code where a given domain is divided into a series of closed rigid blocks bounded by "faults" locked to a defined depth. The observed velocities can be inverted, solving for the Euler vector that best describes the rigid motion of each block, strain accumulation at locked faults, long-term fault slip along block boundaries, and the amount of convergence along the different faults. The model assumes an elastic homogeneous rheology. To represent the tectonic configuration of the region, we use the five blocks defined in the previous section (Fig. 12). All blocks are defined using the

simplified regional fault map presented by Dixon et al. (2002). Faults are considered to be vertical (89° dip to the north or east) and completely locked from the surface down to 20 km depth. Different locking depths (from 10 to 30 km) or dip directions were tested without significantly altering the results presented below. The large difference in the age of the last seismic event between the different faults will not allow the use of this model to correctly partition the slip among the different faults and thus correctly estimate the magnitude of slip on a particular fault (Dixon et al., 2002). Following Savage and Lisowski (1998), different locking depths for different faults could be used to simulate the variable stage of the earthquake cycle. While this method could allow for a better characterization of the fault-slip partitioning among the various faults, the physical relation between locking depth and age since the last earthquake is not straightforward and would increase significantly the number of parameters for the model. We tested shallow locking depth for faults with more recent events (e.g., San Miguel–Vallecitos) and deeper locking depth for faults without historical earthquake (e.g., Agua Blanca). We noticed that while the individual long-term fault rate is changing significantly, for each fault segment, the ratio between fault-parallel and fault-perpendicular motion is only controlled by the block geometry and does not seem to be affected by the strain partition among the different faults. Thus, we choose to simplify or model using a constant locking depth; and in the discussion section below, rather than discuss the magnitude of the long-term rate for each individual fault, we will focus on the relationship between fault-parallel and fault-perpendicular components of the velocity field. In particular, we will focus on the amount of fault-perpendicular strain along the ABF. For this study, the geodetic estimate of fault-perpendicular strain is defined as the heave component of the horizontal slip vector. It is normalized such that the lateral and heave components sum to a total of 100% of the horizontal slip vector. Heave can be expressed as either extension or shortening; but in this study, we find the heave component to be consistently extensional along the entire length of the ABF.

DISCUSSION

Summary of Total Displacements along the ABF

The total horizontal or strike separation measured from mid-Cretaceous structures and intrusions for the ABF and STF in the central and western sections of the fault are shown in Table 4. In Cañon Dolores, we argue that the 10.6 ± 0.5 km offset provided by the western margin of the SMDS is preferred, while the Cretaceous shear zone provides a separation of 11.2 ± 2.0 km in Valle Agua Blanca. In Valle Santo Tomás, offset intrusions along the ABF yield a separation of 4.9 ± 0.2 km. Finally, in the Punta Banda section, the northwestern and southeastern margins of an offset intrusion yield 7.1 ± 2.5 km and 6.3 ± 0.3 km, respectively. However, because this variance likely results from more than a kilometer of northeast-side-down normal dip-slip displacement on the ABF, we prefer the measurement from the midpoints of the intrusions along the fault (tacitly the same as the mean of two margin separations), which yields 6.8 ± 2.8 km. The magnitudes of normal-sense, dip-slip displacements are on the order of a few hundred meters in the Cañon Dolores and Valle Agua Blanca sections (i.e., less than a percent of the displacement). In the Santo Tomás and Punta Banda sections, total dip-slip displacements are estimated to be 1.16 km and 1.25 km, respectively. However, to be able to compare the geologic results with those of the geodetic results properly, we will use the heave, or horizontal component, of displacement. The heave for the STF in the Valle Santo Tomás section was 0.58 km, and that for the ABF in the Punta Banda section was 0.65 km, or 11%–12% of the total slip in the former section and between 7% and 16% for the latter.

Based on the observations from the geodetic modeling and the relative proportions of strike-slip versus total heave on the ABF and STF farther to the northwest (both topics discussed below), we believe it is worth making some speculations concerning the amount of strike-slip motion that may have been

TABLE 4. TOTAL HORIZONTAL SEPARATION OF CRETACEOUS INTRUSIONS AND STRUCTURES

Location and/or feature	Total strike separation (km)	Total heave (km)
Cañon Dolores		
Western margin of the San Marcos dike swarm	10.6 ± 0.5	N/A
Western margins of the K_{RP}-$K_{UQD\text{-}BT}$ (RP-N to RP-S)	11.9 ± 0.2	N/A
Valle Agua Blanca		
Cretaceous shear zone (CSZ-N to CSZ-S)	11.2 ± 2.0	N/A
Valle Santo Tomás		
Agua Blanca fault (ABF): Northwestern margins of K_{EZ}-K_{LA} (EZ-N to EZ-S)	4.9 ± 0.2	N/A
Santo Tomás fault (STF): Estimated range	0.1 to 3.2	0.58
Valle Uruapan		
Northwestern margins of the K_U-K_{LAP} (UP-NW to UP-SW)	7.1 ± 2.5	
Southeastern margins of the K_U-K_{LAP} (UP-NE to UP-SE)	6.3 ± 0.3	
Middle point of the Uruapan and Las Animas plutons	6.8 ± 2.8	0.65

accommodated by the STF. Block modeling suggests that between 7% and 10% of the motion on the ABF system in the Valle Santo Tomás section is normal dip slip. The ABF in Valle Santo Tomás has a preferred displacement of 4.9 ± 0.2 km and motion that is almost perfectly strike parallel. The heave on the STF is ~580 m, which is between 11% and 12% of the total slip determined from the ABF. However, if the range should be between 7% and 10%, then the STF may have between 0.1 and 3.2 km of strike-slip displacement. This would bring the total strike-slip displacement in this section of the ABF to a maximum of 8.3 km. Based on the 3.2 km of strike-slip displacement and a heave of 0.58 km, restoration of this slip would place the point where the central and western STF sections meet (yellow dot labeled B in Fig. 7) and yellow point B′ adjacent to each other. Topographically, this seems like a reasonable fit because it places the salient portion of the ridge front on the southwest adjacent to the recessional part of the ridge on the northeast side of the valley.

The maximum dextral offsets in the Valle Santo Tomás and the Punta Banda sections—8.1 km and 9.6 km, respectively—suggest some slip is transferred onto any of a series of smaller faults present to the northeast of the ABF. These include the Tres Hermanos fault (THF, Fig. 2) and two unnamed faults associated with hot springs located between the ABF and the THF (the southwesternmost is shown [UF] in the southeast corner of Fig. 7). Detailed studies are lacking for these lesser structures.

In summary, dextral strike-slip displacement on the ABF reaches a maximum (10–12 km) in the central sections located in Cañon Dolores and Valle Agua Blanca and decreases toward the west in the Santo Tomás and Punta Banda sections with total slip ranging from ~5–9 km. Our work shows that the ABF is transtensional along its entire length, and the amount of fault perpendicular extension correlates with fault orientation, which is consistent with the interpretations from the block modeling of the geodetic data (see below). An additional component of extensional deformation is required to maintain strain compatibility of the strong slip gradient associated with the eastern terminus of the ABF in Valle Trinidad.

Geodetic Block Modeling

Geodetic block modeling shows that the ABF is transtensional along its entire length (Fig. 12), in agreement with the results from geologic mapping. Little direct geologic evidence of transtension exists for the Cañon Dolores section, which contains the weakest signal at less than 2% fault-perpendicular extension from geodesy. In the Valle Agua Blanca section, geodetic estimates of fault-perpendicular extension rise to 2%–5%, and this segment contains a long, narrow sedimentary basin formed between overlapping fault strands with a pull-apart geometry. Sedimentary basins are present in the Valle Trinidad and Valle Santo Tomás sections, where geodetic extension estimates vary from 5% to 10%. Lastly, in the Punta Banda section, where geodetic estimates of fault perpendicular extension rise to 10%–13%, the ABF becomes more strongly oblique, and its finite slip has more than 1 km of normal-sense dip-slip displacement. These largest estimates of fault-perpendicular extension are associated with the largest sedimentary basin that hosts the vast agricultural enterprises of Maneadero and the more extensive Bahía Todos Santos marine basin. In summary, the comparisons between geodetic and geologic estimates of fault-normal extension in the Valle Santo Tomás and Punta Banda sections are within error of each other.

Regional Implications

The ABF is the northern limit of the rigid Baja California microplate, which, as demonstrated by Plattner et al. (2007), is strongly coupled with the Pacific plate, ~90% of the relative motion between the Pacific and North American plates being accommodated within the Gulf of California. Consequently, only a small fraction (3–4 mm/yr) of the plate-boundary shear is accommodated on the San Benito, San Lazaro–Santa Margarita, and the Tosco-Abreojos fault systems (e.g., Spencer and Normark, 1979; Dixon et al., 2000; Michaud et al., 2004; Fletcher et al., 2007) present between the Pacific plate and the Baja California microplate south of Punta China (Fig. 2). In contrast, offshore faults of the continental borderlands domain to the north of Punta Banda, where the ABF goes offshore, are estimated to accommodate ~20% of the plate-boundary shear, with perhaps as much as 10–11 mm/yr of slip (DeMets and Dixon, 1999; Ryan et al.,. 2009). Based on our geodetic results, some of the additional 6–8 mm/yr is derived from the Agua Blanca–Santo Tomás–Maximinos fault network.

Geologic and geodetic observations and geodetic modeling demonstrate that relative to the disrupted northern part of the Baja California microplate north of the ABF, motion of the rigid Baja California microplate is essentially parallel to the fault through the Cañon Dolores section (i.e., ~276°). However, this motion is misaligned with the Baja California microplate's motion relative to North America. The relative magnitude of the component of the microplate's motion that is parallel to NrB–North American motion can be calculated as the difference between the NrB and North American Euler poles, both with respect to IGS08 (Table 2). This yields a vector with a direction of 320°, or ~44° clockwise from 276°. If we assume that the 6 mm/yr slip rate determined for the ABF in Valle Agua Blanca (Rockwell et al., 1993) is accurate and toward 276°, then ~4.2 mm/yr, or ~70%, of the slip carried by the ABF is parallel to the North American–rigid Baja California microplate and Pacific plate boundary shear. Thus, this amount is ultimately transferred out of the Gulf and onto the faults of the Inner Continental Borderlands.

It is possible that the anomalous westerly orientation and transtensional kinematics of the ABF are related to perturbations of the expected regional stress state. One possible perturbation could be related to the partitioning of extensional deformation in this portion of the plate margin. To the east, extensional deformation associated with of the San Pedro Mártir fault and a related series of detachment faults in the Sierra San Felipe (Seiler et al., 2010, 2011; Rossi et al., 2017) is located largely to the south of the eastward projection of the ABF. North of this projection in the southern Sierra Juarez, however, the

magnitude of extension is dramatically less (e.g., Lee et al., 1996). Offshore to the west of Baja California, extensional deformation in the continental borderland is located largely to the north of the westward projection of the ABF (Legg et al., 1991; Ryan et al., 2009). Therefore, as was first proposed by Hamilton (1971), the ABF may be acting as a transfer structure between these two offset zones of plate margin extension. The differences between the transtensional deformation along eastern and western sections of the fault, but the relative lack of it in central sections, suggest the origin of this extensional component results from changes in the orientation of the ABF.

Fletcher et al. (2014) proposed that the observed transtension throughout the southern BBD demonstrates that stress related to gravitational potential energy (GPE) gradient generated by the collapse of the Great Basin (Jones et al., 1996; Flesch et al., 2000) is not transmitted all the way across the BBD. Although this must be true, it does not resolve the problem because the sense of fault-normal deformation on the ABF is opposite to that expected if relative plate motion were the only factor controlling the orientation and kinematics of faulting. However, GPE associated with the uplifted Main Gulf Escarpment and lithospheric removal from below the eastern Peninsular Ranges could be contributing to the westward motion of the rigid Baja California microplate similar to the role that the GPE gradients play in the Basin and Range and Sierra Nevada block motion.

The location and orientation of the ABF have been suggested by some past studies, including some by authors here, to have been controlled by preexisting structures such as the Cretaceous shear zone used to constrain the total offset in Valle Agua Blanca (e.g., Gastil et al., 1981). We argue that this is an unlikely explanation because ABF cuts the older thrust fault at a high angle (40°–80°) in Valle Agua Blanca and would have projected above the fault for the western third of its trace. Therefore, the reactivation of a preexisting fabric cannot be used to explain the mechanical misorientation of the ABF with respect to both far-field relative motion and regional maximum compressive stress, which form angles of 37°–67° to its trace. Alternatively, we propose that its orientation is instead controlled by the extensional domains that it connects in the borderland to the west and Gulf of California to the east.

The geologic data presented here cannot produce a unique timing of fault initiation. However, given available slip-rate determinations and total offsets, as well as potential relations with other faults in this part of the BBD, we believe we can draw some conclusions regarding the timing of initial displacement on ABF. Rockwell et al. (1993) report late Quaternary slip rates of 3.2 ± 0.9 mm/yr for the Punta Banda section of the ABF and 6 ± 1 mm/yr for the Valle Agua Blanca section, where total displacements are measured at 6.3 ± 0.3 km and 11.2 ± 2.0 km, respectively. Based solely on these numbers, and the tenuous assumption that the slip velocities of the ABF have remained constant throughout its history, the ABF could have initiated between ca. 1.5 and 3.3 Ma. The lower bound would place its initiation close to that of the Elsinore, San Felipe, and the San Jacinto faults in the northeastern part of the SCSZ (Steely et al., 2009; Janecke et al., 2010; Dorsey et al., 2012). However, as several recent studies have demonstrated (e.g., Janecke et al., 2010; McGill et al., 2013; Onderdonk et al., 2015), the slip rates of individual faults, particularly those within networks of faults, such as the ECSZ and the SCSZ, are prone to significant variations throughout their evolutions, including a period of initial acceleration (e.g., Gourmelen et al., 2011). Thus, these initiation ages, particularly the age of ca. 1.5 Ma, are best considered to represent absolute minimums.

CONCLUSIONS

The ABF is a west-northwest–trending oblique dextral-normal fault that defines the southern boundary of the BBD (Fig. 1) and juxtaposes the disrupted northernmost part of the Baja California microplate with the rigid portion to the south. Results from geologic and geodetic studies demonstrate that the amount of total dextral displacement on the ABF is at a maximum of ~11 km in the central portions of the fault where motion is nearly all strike-parallel. However, the magnitude of displacement decreases and the proportion of the dip-slip component increases to both the east and west. To the east, the ABF appears to die out before crossing into the San Pedro Mártir fault, with slip being transferred onto a series of more northerly-trending, dip-slip faults. The western third of the ABF, including both the Santo Tomás and Punta Banda sections, exhibits between 5 and 9 km of dextral offset and 0.58 km of heave on the STF in the Valle Santo Tomás section and 0.65 km of heave on the ABF in the Punta Banda section. Small offset faults proximal to the ABF (e.g., THF) likely accommodate much of the missing dextral shear in these sections of the ABF.

Geodetic data and block modeling provide consistent results with those from the geologic component of this study. These results indicate block motion that is in near perfect alignment with the central ABF and increased proportions of extensional dip-slip motion to both the east (3%–10%) and west (5%–13%).

The west-northwest motion of the rigid Baja California microplate is derived, at least in part, from the extensional collapse within the Gulf extensional corridor at the east end of the fault. The ABF, as suggested by Warren Hamilton (Hamilton, 1971), serves as a transfer structure connecting regions of extension on both sides of the Baja Peninsula.

Finally, based on the total offsets and slip rates reported here and by others for the ABF, we suggest that the fault likely initiated between 3.3 and 1.5 Ma. This age range overlaps with those reported for other faults to the southwest of the SAF within the BBD.

REFERENCES CITED

Allen, C., Silver, L., and Stehil, F., 1960, Agua Blanca fault—A major transverse structure of northern Baja California, Mexico: Geological Society of America Bulletin, v. 71, p. 467–482, https://doi.org/10.1130/0016-7606(1960)71[467:ABFMTS]2.0.CO;2.

Allison, E.C., 1974, The type Alisitos Formation (Cretaceous, Aptian–Albian) of Baja California and its bivalve fauna, *in* Gastil, R.G., and Lillegraven, J., eds., A Guidebook to the Geology of Peninsular California: American Association of Petroleum Geologists, Pacific Section, Field Trip Guidebook, Joint Annual Spring Meeting of the American Association of Petroleum

Geologists, Pacific Section; Society of Economic Paleontologists and Mineralogists, Pacific Section; and Society of Exploration Geophysicists, April 1974, no. 49, p. 20–59.
Alsleben, H., Wetmore, P.H., Schmidt, K.L., Paterson, S.R., and Melis, E.A., 2008, Complex deformation during arc-continent collision: Quantifying finite strain in the accreted Alisitos arc, Peninsular Ranges batholith, Baja California: Journal of Structural Geology, v. 30, p. 220–236, https://doi.org/10.1016/j.jsg.2007.11.001.
Alsleben, H., Wetmore, P.H., Gehrels, G.E., and Paterson, S.R., 2011, Detrital zircon ages in Paleozoic and Mesozoic basement assemblages of the Peninsular Ranges batholith, Baja California, Mexico: Constraints for depositional ages and provenance: International Geology Review, v. 54, no. 1, p. 93–110, https://doi.org/10.1080/00206814.2010.509158.
Alsleben, H., Wetmore, P.H., and Paterson, S.R., 2014, Structural evidence of mid-Cretaceous suturing of the Alisitos arc to North America from the Sierra Calamajue, Baja California, Mexico, *in* Morton, D.M., and Miller, F.K., eds., Peninsular Ranges Batholith, Baja California and Southern California: Geological Society of America Memoir 211, p. 691–711, https://doi.org/10.1130/2014.1211(22).
Bassiri, S., and Hajj, G.A., 1993, Higher-order ionospheric effects on the global positioning systems observables and means of modeling them: Manuscripta Geodetica, v. 18, p. 280–289.
Bennett, R.A., Rodi, W., and Reilinger, R.E., 1996, Global positioning system constraints on fault slip rates in southern California and northern Baja, Mexico: Journal of Geophysical Research, v. 101, p. 21,943–21,960, https://doi.org/10.1029/96JB02488.
Bertiger, W., Desai, S.D., Haines, B., Harvey, N., Moore, A.W., Owen, S., and Weiss, J.-P., 2010, Single receiver phase ambiguity resolution with GPS data: Journal of Geodesy, v. 84, p. 327–337, https://doi.org/10.1007/s00190-010-0371-9.
Cage, W.R., 2010, Geomorphic mapping and ground-penetrating radar survey of the Agua Blanca fault in Valle de Santo Tomás, Baja California, Mexico [M.S. thesis]: Fort Worth, Texas, Texas Christian University, 92 p.
Callihan, S., 2010, Constraining the geometry and evolution of the Maneadero basin, Baja California, Mexico [M.S. thesis]: Tampa, Florida, University of South Florida, 67 p.
Crowell, J.C., 1982, The tectonics of Ridge Basin, southern California, *in* Crowell, J.C. and Link, M.H., eds., Geologic History of Ridge Basin, Southern California: Los Angeles, Pacific Section, Society of Economic Paleontologists and Mineralogists, Book 22, p. 25–42.
Crowell, J.C., 2003, Tectonics of ridge Basin region, southern California, *in* Crowell, J.C., ed., Evolution of Ridge Basin, Southern California: An Interplay of Sedimentation and Tectonics: Geological Society of America Special Paper 367, p. 157–203, https://doi.org/10.1130/0-8137-2367-1.157.
DeMets, C., and Dixon, T.H., 1999, New kinematic models for Pacific–North America motion from 3 Ma to Present, 1: Evidence for steady motion and biases in the NUVEL-1A model: Geophysical Research Letters, v. 26, p. 1921–1924, https://doi.org/10.1029/1999GL900405.
Dixon, T.H., Farina, F., DeMets, C., Suarez-Vidal, F., Fletcher, J., Margquez-Azua, B., Miller, M., Sanchez, O., and Umhoefer, P., 2000, New kinematic models for Pacific–North America motion from 3 Ma to Present, II: Evidence for a Baja California shear zone: Geophysical Research Letters, v. 27, p. 3961–3964, https://doi.org/10.1029/2000GL008529.
Dixon, T.H., Decaix, J., Farina, F., Furlong, K., Malservisi, R., Bennett, R., Suarez-Vidal, F., Fletcher, J., and Lee, J., 2002, Seismic cycle and rheological effects on estimation of present-day slip rates for the Agua Blanca and San Miguel–Vallecitos faults, northern Baja California, Mexico: Journal of Geophysical Research, v. 107, https://doi.org/10.1029/2000JB000099.
Dorsey, R.J., Axen, G.J., Peryam, T.C., and Kairouz, M.E., 2012, Initiation of the southern Elsinore fault at ~1.2 Ma: Evidence from the Fish Creek–Vallecito Basin, southern California: Tectonics, v. 31, no. 2, TC2006, https://doi.org/10.1029/2011TC003009.
Doser, D., 1992, Faulting processes of the 1956 San Miguel, Baja California earthquakes: Pure and Applied Geophysics, v. 139, p. 3–16, https://doi.org/10.1007/BF00876824.
Farquharson, P.T., 2004, Geology of the Rancho San Marcos dike swarm, Baja California, Mexico [M.S. thesis]: San Diego, California, San Diego State University, 79 p.
Fisher, M.A., Sorlien, C.C., and Sliter, R.W., 2009, Potential earthquake faults offshore southern California, from the eastern Santa Barbara Channel south to Dana Point, *in* Lee, H.J., and Normark, W.R., eds., Earth Science in the Urban Ocean: The Southern California Continental Borderland: Geological Society of America Special Paper 454, p. 271–290, https://doi.org/10.1130/2009.2454(4.4).
Flesch, L.M., Holt, W.E., Haines, A.J., and Shen-Tu, B., 2000, Dynamics of the Pacific–North American plate boundary in the western United States: Science, v. 287, p. 834–836, https://doi.org/10.1126/science.287.5454.834.
Fletcher, J.M., and Spelz, R.M., 2009, Patterns of Quaternary deformation and rupture propagation associated with an active low-angle normal fault, Laguna Salada, Mexico: Evidence for a rolling hinge?: Geosphere, v. 5, p. 385–407, https://doi.org/10.1130/GES00206.1.
Fletcher, J.M., Grove, M., Kimbrough, D., Lovera, O., and Gehrels, G.E., 2007, Ridge-trench interactions and the Neogene tectonic evolution of the Magdalena shelf and southern Gulf of California: Insights from detrital zircon U-Pb ages from the Magdalena fan and adjacent areas: Geological Society of America Bulletin, v. 119, p. 1313–1336, https://doi.org/10.1130/B26067.1.
Fletcher, J.M., Teran, O.J., Rockwell, T.K., Oskin, M.E., Hudnut, K.W., Mueller, K.J., Spelz, R.M., Akciz, S.O., Masana, E., Faneros, G., Fielding, E.J., Leprince, S., Morelan, A.E., Stock, J., Lynch, D.K., Elliott, A.J., Gold, P.O., Liu-Zeng, J., González-Ortega, A., Hinojosa-Corona, A., and González-García, J., 2014, Assembly of a large earthquake from a complex fault system: Surface rupture kinematics of the 4 April 2010 El Mayor–Cucapah (Mexico) Mw 7.2 earthquake: Geosphere, v. 10, p. 797–827, https://doi.org/10.1130/GES00933.1.
Gastil, R.G., 1993, Prebatholithic history of Peninsular California, *in* Gastil, R.G., and Miller, H., eds., The Prebatholithic Stratigraphy of Peninsular California: Geological Society of America Special Paper 279, p. 145–156, https://doi.org/10.1130/SPE279-p145.
Gastil, R.G., Phillips, R., and Allison, E., 1975, Reconnaissance Geology of the State of Baja California: Geological Society of America Memoir 140, 170 p, https://doi.org/10.1130/MEM140-p1.
Gastil, R.G., Morgan, G.J., and Krummenacher, D., 1981, The tectonic history of peninsular California and adjacent Mexico, *in* Ernst, W.G., ed., The Geotectonic Development of California (Rubey Volume I): Englewood Cliffs, New Jersey, Prentice-Hall, p. 284–306.
Gonzalez-Ortega, A., Fialko, Y., Sandwell, D., Nava-Pichardo, F.A., Fletcher, J., Gonzalez-Garcia, J., Lipovsky, B., Floyd, M., and Funning, G., 2014, El Mayor–Cucapah (Mw 7.2) earthquake: Early near-field postseismic deformation from InSAR and GPS observations: Journal of Geophysical Research, v. 119B, p. 1482–1497, https://doi.org/10.1002/2013JB010193.
Gourmelen, N., Dixon, T.H., Amelung, F., and Schmalzle, G., 2011, Acceleration and evolution of faults: An example from the Hunter Mountain–Panamint Valley fault zone, eastern California: Earth and Planetary Science Letters, v. 301, p. 337–344, https://doi.org/10.1016/j.epsl.2010.11.016.
Hackl, M., Malservisi, R., Hugentobler, U., and Wonnacott, R., 2011, Estimation of velocity uncertainties from GPS time series: Examples from the analysis of the South African TrigNet network: Journal of Geophysical Research, v. 116, B11404, https://doi.org/10.1029/2010JB008142.
Hackl, M., Malservisi, R., Hugentobler, U., and Jiang, Y., 2013, Velocity covariance in the presence of anisotropic time correlated noise and transient events in GPS time series: Journal of Geodynamics, v. 72, p. 36–45, https://doi.org/10.1016/j.jog.2013.08.007.
Hamilton, W., 1971, Recognition on space photographs of structural elements of Baja California: U.S. Geological Survey Professional Paper 718, 32 p., https://doi.org/10.3133/pp718.
Hatch, M.E., 1987, Neotectonics of the Agua Blanca fault, Valle Agua Blanca, Baja California, Mexico [M.S. thesis]: San Diego, California, San Diego State University, 94 p.
Heidbach, O., Tingay, M., Barth, A., Reinecker, J., Kurfeß, D., Muller, B., 2010, World Stress Map 1–1: Paris, Commission for the Geological Map of the World, scale 1:46,000,000, https://doi.org/10.1594/GFZ.WSM.Map2009.
Herring, T.A., Melbourne, T.I., Murray, M.H., Floyd, M.A., Szeliga, W.M., King, R.W., Phillips, D.A., Puskas, C.M., Santillan, M., and Wang, L., 2016, Plate Boundary Observatory and related networks: GPS data analysis methods and geodetic products: Reviews of Geophysics, v. 54, p. 759–808, https://doi.org/10.1002/2016RG000529.
Herzig, C.T., and Kimbrough, D.L., 2014, Santiago Peak volcanics: Early Cretaceous arc volcanism of the western Peninsular Ranges batholith, southern California, *in* Morton, D.M., and Miller, F.K., eds., Peninsular Ranges Batholith, Baja California and Southern California: Geological Society of America Memoir 211, p. 345–363, https://doi.org/10.1130/2014.1211(09).
Herzog, D.W., 1998, Subsurface structural evolution along the northern Wittier fault zone of the eastern Las Angeles Basin, southern California, [M.S. thesis]: Corvallis, Oregon, Oregon State University, 64 p.
Hilinski, T.E., 1988, Structure and Quaternary faulting about the eastern terminus of the Agua Blanca fault, Baja California, Mexico [M.S. thesis]: San Diego, California, San Diego State University, 91 p.
Hill, M.L., and Dibblee, T.W., 1953, San Andreas, Garlock, and Big Pine faults, California a study of the character, history, and tectonic significance of their displacements: Geological Society of America Bulletin, v. 64, p. 443–458, https://doi.org/10.1130/0016-7606(1953)64[443:SAGABP]2.0.CO;2.

Hirabayashi, C.K., Rockwell, T.K., Wesnousky, S.G., Stirling, M.W., and Suarez-Vidal, F., 1996, A neotectonic study of the San Miguel-Vallecitos fault, Baja California, Mexico: Bulletin of the Seismological Society of America, v. 86, p. 1770–1783.

Ingersoll, R.V., and Rumelhart, P.E., 1999, Three-stage evolution of the Los Angeles basin, southern California: Geology, v. 27, p. 593–596, https://doi.org/10.1130/0091-7613(1999)027<0593:TSEOTL>2.3.CO;2.

Janecke, S.U., Dorsey, R.J., Forand, D., Steely, A.N., Kirby, S.M., Lutz, A.T., Housen, B.A., Langenheim, V.E., and Rittenour, T.M., 2010, High Geologic Slip Rates since Early Pleistocene Initiation of the San Jacinto and San Felipe Fault Zones in the San Andreas Fault System: Southern California, USA: Geological Society of America Special Paper 475, 48 p., https://doi.org/10.1130/2010.2475.

Jones, C.H., Unruh, J.R., and Sonder, L.J., 1996, The role of gravitational potential energy in active deformation in the southwestern United States: Nature, v. 381, p. 37–41, https://doi.org/10.1038/381037a0.

Kedar, S., Hajj, G.A., Wilson, B.D., and Heflin, M.B., 2003, The effect of the second order GPS ionospheric correction on receiver positions: Geophysical Research Letters, v. 30, 1829, https://doi.org/10.1029/2003GL017639.

Kellogg, K.S., and Minor, S.A., 2005, Pliocene transpressional modification of depositional basins by convergent thrusting adjacent to the "Big Bend" of the San Andreas fault: An example from Lockwood Valley, southern California: Tectonics, v. 24, no. 1, https://doi.org/10.1029/2003TC001610.

Kremer, C., Hammond, W.C., and Blewitt, G., 2018, A robust estimation of the 3-D intraplate deformation of the North American plate from GPS: Journal of Geophysical Research: Solid Earth, v. 123, no. 5, p. 4388–4412, https://doi.org/10.1029/2017JB015257.

Kretzer, C.S., 2010, Geologic mapping and ground-penetrating radar surveys of the Valle Santo Tomás segment of the Agua Blanca fault, Baja California, Mexico [M.S. thesis]: Fort Worth, Texas, Texas Christian University, 68 p.

Lee, J., Miller, M.M., Crippen, R., Hacker, B., and Ledesma-Vazquez, J., 1996, Middle Miocene extension in the Gulf Extensional Province, Baja California: Evidence from the southern Sierra Juarez: Geological Society of America Bulletin, v. 108, p. 505–525, https://doi.org/10.1130/0016-7606(1996)108<0505:MMEITG>2.3.CO;2.

Legg, M.R., 1985, Geologic structure and tectonics of the inner continental borderland offshore northern Baja California, Mexico [Ph.D. thesis]: Santa Barbara, California, University of California, Santa Barbara, 410 p.

Legg, M.R., Wong, O.V., and Suarez-Vidal, F., 1991, Geologic structure and tectonics of the inner continental borderland of northern Baja California, *in* Dauphin, J.P.E., and Simoneit, B.R.T., eds., The Gulf and Peninsular Province of the Californias: Tulsa, Oklahoma, American Association of Petroleum Geologists Memoir 47, p. 145–177.

Madsen, S.R., 2009, Geomorphic mapping and ground-penetrating radar survey of the western segment of the Agua Blanca fault, Baja California, Mexico [M.S. thesis]: Fort Worth Texas, Texas Christian University, 96 p.

Malservisi, R., Ugentobler, U., Wonnacott, R., and Hackl, M., 2013, How rigid is a rigid plate?: Geodetic constraint from the TrigNet CGPS network, South Africa: Geophysical Journal International, v. 192, p. 918–928, https://doi.org/10.1093/gji/ggs081.

Mao, A., Harrison, C.G.A., and Dixon, T.H., 1999, Noise in GPS coordinate time series: Journal of Geophysical Research, v. 104, no. B2, p. 2797–2816, https://doi.org/10.1029/1998JB900033.

McCaffrey, R., 2002, Crustal block rotations and plate coupling, *in* Stein, S., and Freymueller, J., eds., Plate Boundary Zones: American Geophysical Union, Geodynamics Series v. 30, p. 101–122.

McGill, S.F., Owen, L.A., Weldon, R.J., II, and Kendrick, K.J., 2013, Latest Pleistocene and Holocene slip rate for the San Bernardino strand of the San Andreas fault, Plunge Creek, Southern California: Implications for strain partitioning within the southern San Andreas fault system for the last ~35 k.y: Geological Society of America Bulletin, v. 125, p. 48–72, https://doi.org/10.1130/B30647.1.

Michaud, F., Sosson, M., Royer, J.Y., Chabert, A., Bourgois, J., Calmus, T., Mortera, C., Bigot-Cormier, F., Bandy, W., Dyment, J., Pontoise, B., and Sichler, B., 2004, Motion partitioning between the Pacific plate, Baja California, and the North American plate: The Tocso-Abreojos fault revisited: Geophysical Research Letters, v. 31, L08604, https://doi.org/10.1029/2004GL019665.

Morton, D.M., and Miller, F.K., 2014, Peninsular Ranges Batholith, Baja California and southern California: Geological Society of America Memoir 211, 758 p., https://doi.org/10.1130/MEM211.

Muehlberger, W.R., 1996, Tectonic map of North America: Tulsa, Oklahoma, American Association of Petroleum Geologists, scale 1:5,000,000.

Mueller, K.J., and Rockwell, T.K., 1995, Late Quaternary activity of the Laguna Salada fault in northern Baja California, Mexico: Geological Society of America Bulletin, v. 107, p. 8–18, https://doi.org/10.1130/0016-7606(1995)107<0008:LQAOTL>2.3.CO;2.

Onderdonk, N.W., McGill, S., and Rockwell, T.K., 2015, Short-term variations in slip rate and size of prehistoric earthquakes during the past 2000 years on the northern San Jacinto fault zone, a major plate-boundary structure in southern California: Lithosphere, v. 7, no. 3, p. 211–234, https://doi.org/10.1130/L393.1.

Oskin, M., and Stock, J., 2003, Cenozoic volcanism and tectonics of the continental margins of the Upper Delfin basin, northeastern Baja California and western Sonora: Geological Society of America Bulletin, v. 115, p. 1173–1190, https://doi.org/10.1130/B25154.1.

Plattner, C., Malservisi, R., Dixon, T., LaFemina, P., Sella, G.F., Fletcher, J., and Suarez-Vidal, F., 2007, New constraints on relative motion between the Pacific Plate and Baja California microplate (Mexico) from GPS measurements: Geophysical Journal International, v. 170, p. 1373–1380, https://doi.org/10.1111/j.1365-246X.2007.03494.x.

Plattner, C., Malservisi, R., and Groves, R., 2009, On plate boundary forces that drive and resist Baja California motion: Geology, v. 37, p. 359–362, https://doi.org/10.1130/G25360A.1.

Plattner, C., Malservisi, R., Amelung, F., Dixon, T.H., Hackl, M., Verdecchia, A., Lonsdale, P., Suarez-Vidal, F., and Gonzalez-Garcia, J., 2015, Space geodetic observation of the deformation cycle across the Ballenas Transform, Gulf of California: Journal of Geophysical Research: Solid Earth, v. 120, no. 8, p. 5843–5862, https://doi.org/10.1002/2015JB011959.

Rebischung, P., Griffiths, J., Ray, J., Schmid, R., Collilieux, X., and Garayt, B., 2012, IGS08: The IGS realization of ITRF2008: GPS Solutions, v. 16, p. 483–494, https://doi.org/10.1007/s10291-011-0248-2.

Rockwell, T.K., 1983, Soil, chronology, geology, and Neotectonics of the north-central Ventura Basin, California [Ph.D. thesis]: Santa Barbara, California, University of California at Santa Barbara, 424 p.

Rockwell, T.K., Hatch, M.E., and Schug, D.L., 1987, Late Quaternary rates: Agua Blanca and Borderlands faults: Reston, Virginia, U.S. Geological Survey Final Technical Report, 122 p.

Rockwell, T.K., Muhs, D.R., Kennedy, G.L., Hatch, M.E., Wilson, S.M., and Klinger, R.E., 1989, Uranium-series ages, faunal correlations and tectonic deformation of marine terraces within the Agua Blanca fault zone at Punta Banda, northern Baja California, Mexico, *in* Abbott, P.L., ed., Geologic Studies in Baja California: Los Angeles, Society of Economic Paleontologists and Mineralogists (Pacific Section), Book 63, p. 1–16.

Rockwell, T.K., Schug, D.L., and Hatch, M.E., 1993, Late Quaternary slip rates along the Agua Blanca fault, Baja California, Mexico, *in* Abbott, P.L., ed., Geological Investigations of Baja California: South Coast Geological Society, Annual Trip Guidebook, no. 21, p. 53–92.

Rossi, M.W., Quigley, M.C., Fletcher, J.M., Whipple, K.X., Diaz-Torres, J.J., Seiler, C., Fifield, L.K., and Heimsath, A.M., 2017, Along-strike variation in catchment morphology and cosmogenic denudation rates reveal the pattern and history of footwall uplift, Main Gulf Escarpment, Baja California: Geological Society of America Bulletin, v. 129, p. 837–854, https://doi.org/10.1130/B31373.1.

Ryan, H.F., Legg, M.R., Conrad, J.E., and Liter, R.W., 2009, Recent faulting in the Gulf of Santa Catalina: San Diego to Dana Point, *in* Lee, H.J., and Normark, W.R., eds., Earth Science in the Urban Ocean: The Southern California Continental Borderland: Geological Society of America Special Paper 454, p. 291–315, https://doi.org/10.1130/2009.2454(4.5).

Savage, J.C., and Lisowski, M., 1998, Viscoelastic coupling model of the San Andreas fault along the big bend, southern California: Journal of Geophysical Research, v. 103, p. 7281–7292, https://doi.org/10.1029/98JB00148.

Schmidt, K.L., Wetmore, P.H., Alsleben, H., and Paterson, S.R., 2014, Mesozoic tectonic evolution of the southern Peninsular Ranges batholith, Baja California, Mexico: Long-lived history of a collisional segment in the Mesozoic Cordilleran arc, *in* Morton, D.M., and Miller, F.K., eds., Peninsular Ranges Batholith, Baja California and Southern California: Geological Society of America Memoir 211, p. 645–668, https://doi.org/10.1130/2014.1211(20).

Schug, D.L., 1987, Neotectonics of the western reach of the Agua Blanca fault, Baja California, Mexico, [M.S. thesis]: San Diego, California, San Diego State University, 128 p.

Seiler, C., Fletcher, J.M., Quigley, M.C., Gleadow, A.J.W., and Kohn, B.P., 2010, Neogene structural evolution of the Sierra San Felipe, Baja California: Evidence for proto-gulf transtension in the Gulf Extensional Province?: Tectonophysics, v. 488, p. 87–109, https://doi.org/10.1016/j.tecto.2009.09.026.

Seiler, C., Fletcher, J.M., Kohn, B.P., Gleadow, A.J.W., and Raza, A., 2011, Low-temperature thermochronology of northern Baja California, Mexico: Decoupled slip-exhumation gradients and

delayed onset of oblique rifting across the Gulf of California: Tectonics, v. 30, https://doi.org/10.1029/2009TC002649.

Silver, L.T., and Chappell, B.W., 1988, The Peninsular Ranges Batholith: An insight into the evolution of the Cordilleran batholiths of southwestern North America: Transactions of the Royal Society of Edinburgh, v. 79, p. 105–121, https://doi.org/10.1017/S0263593300014152.

Silver, L.T., Stehli, G.G., and Allen, C.R., 1963, Lower Cretaceous pre-batholithic rocks of northern Baja California, Mexico: American Association of Petroleum Geologists Bulletin, v. 47, p. 2054–2059.

Spencer, J.E., and Normark, W., 1979, Tosco-Abreojos fault zone: A Neogene transform plate boundary within the Pacific margin of southern Baja California, Mexico: Geology, v. 7, p. 554–557, https://doi.org/10.1130/0091-7613(1979)7<554:TFZANT>2.0.CO;2.

Springer, A., 2010, Constraining basin geometry and fault kinematics on the Santo Tomás segment of the Agua Blanca fault through a combined geophysical and structural study [M.S. thesis]: Tampa, Florida, University of South Florida, 58 p.

Steely, A.N., Janecke, S.U., Dorsey, R.J., and Axen, G.J., 2009, Early Pleistocene initiation of the San Felipe fault zone, SW Salton Trough, during reorganization of the San Andreas fault system: Geological Society of America Bulletin, v. 121, p. 663–687, https://doi.org/10.1130/B26239.1.

Suarez-Vidal, F., Armijo, R., Morgan, G., Bodin, P., and Gastil, R.G., 1991, Framework of recent and active faulting in northern Baja California, *in* Dauphin, J.P.E., and Simoneit, B.R.T., eds., The Gulf and Peninsular Province of the Californias: Tulsa, Oklahoma, American Association of Petroleum Geologists Memoir 47, p. 285–300.

Townend, J., and Zoback, M.D., 2004, Regional tectonic stress near the San Andreas fault in central and southern California: Geophysical Research Letters, v. 31, https://doi.org/10.1029/2003GL018918.

U.S. Geological Survey, 2006, Quaternary fault and fold database for the United States: http://earthquake.usgs .gov/regional/qfaults/.

Walawender, M.J., Gastil, R.G., Clinkenbeard, J.P., McCormick, W.V., Eastman, B.G., Wernicke, R.S., Wardlaw, M.S., and Smith, B.M., 1990, Origin and evolution of the zoned La Posta-type plutons, eastern Peninsular Ranges batholith of southern and Baja California, *in* Anderson, J.L., ed., The Nature and Origin of Cordilleran Magmatism: Boulder Colorado, Geological Society of America Memoir, v. 174, p. 1–18, https://doi.org/10.1130/MEM174-p1.

Walawender, M.J., Girty, G.H., Lombardi, M.R., Kimbrough, D., Girty, M.S., and Anderson, C., 1991, A synthesis of recent work in the Peninsular Ranges batholith, *in* Walawender, M.J., and Hanan, B.B., eds., Geological Excursions in Southern California and Mexico: Fieldtrip Guidebook and Volume for the Joint Meeting of the Cordilleran Section, Geological Society of America and Pacific Section American Association of Petroleum Geologists, Society for Sedimentary Geology, p. 297–318.

Wdowinski, S., Smith-Konter, B., Bock, Y., and Sandwell, D., 2007, Diffuse interseismic deformation across the Pacific–North American plate boundary: Geology, v. 35, p. 311–314, https://doi.org/10.1130/G22938A.1.

Wetmore, P.H., Schmidt, K.L., Paterson, S.R., and Herzig, C., 2002, Tectonic implications for the along-strike variation of the Peninsular Ranges batholith, southern and Baja California: Geology, v. 30, p. 247–250, https://doi.org/10.1130/0091-7613(2002)030<0247:TIFTAS>2.0.CO;2.

Wetmore, P.H., Herzig, C., Schultz, P.W., Alsleben, H., Paterson, S.R., and Schmidt, K.L., 2003, Mesozoic tectonic evolution of the Peninsular Ranges of southern Baja California, *in* Johnson, S.E., Paterson, S.R., Fletcher, J.M., Girty, G.H., Kimbrough, D.L., and Martin-Barajas, A., eds., Tectonic Evolution of Northwestern Mexico and the Southwestern USA: Geological Society of America Special Paper 374, p. 93–116, https://doi.org/10.1130/0-8137-2374-4.93.

Wetmore, P.H., Alsleben, H., Paterson, S.R., Ducea, M.N., Gehrels, G.E., and Valencia, V.A., 2005, Field trip to the northern Alisitos arc segment: Ancestral Agua Blanca fault region: Ensenada, Baja California, Mexico, Field Conference Guidebook for the VII International Meeting of the Peninsular Geological Society, 39 p.

Wetmore, P.H., Hughes, S.S., Stremtan, C., Ducea, M.N., and Alsleben, H., 2014, Tectonic implications of postcontractional magmatism of the Alisitos arc segment of the Peninsular Ranges, Baja California, Mexico, *in* Morton, D.M., and Miller, F.K., eds., Peninsular Ranges Batholith, Baja California and Southern California: Geological Society of America Memoir 211, p. 669–690, https://doi.org/10.1130/2014.1211(21).

Yeats, R.S., Huftile, G.J., and Stitt, L.T., 1994, Late Cenozoic tectonics of the east Ventura basin, Transverse Ranges, California: American Association of Petroleum Geologists Bulletin, v. 78, p. 1040–1074.

Zumberge, J.F., Heflin, M.B., Jefferson, D.C., Watkins, M.M., and Webb, F.H., 1997, Precise point positioning for the efficient and robust analysis of GPS data from large networks: Journal of Geophysical Research, v. 102, no. B3, p. 5005–5017, https://doi.org/10.1029/96JB03860.